Supporting Information

for

Methodology to Relate Black Carbon Particle Number and Mass Emissions

Roger Teoh[1], Marc E.J. Stettler[1]*, Arnab Majumdar[1], Ulrich Schumann[2], Brian Graves[3] and Adam Boies[3]

[1] Centre for Transport Studies, Department of Civil and Environmental Engineering, Imperial College London, London, SW7 2AZ, United Kingdom

[2] Deutsches Zentrum für Luft- und Raumfahrt, Institute of Atmospheric Physics, 82234 Oberpfaffenhofen, Germany

[3] Department of Engineering, University of Cambridge, Cambridge, CB2 1PZ, United Kingdom

* Corresponding author. E-mail address: m.stettler@imperial.ac.uk

S1 – DERIVATION OF THE NEW FRACTAL AGGREGATE (FA) MODEL

S1.1 Simplified Derivation of the FA Model (Eq. 15, main text) excluding C_{ov}

Derivation of $N = \frac{M}{k_a \rho_0 (\frac{\pi}{6})(k_{\mathrm{TEM}})^{3-2D_\alpha} \mathrm{GMD}^{\varphi} \exp(\frac{\varphi^2 \ln(\mathrm{GSD})^2}{2})}$ where $\varphi = 3D_{\mathrm{TEM}} + (1 - D_{\mathrm{TEM}})2D_\alpha$

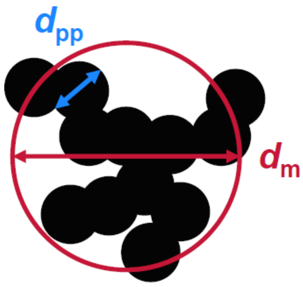

Figure S1: Graphical illustration of one BC aggregate consisting of many smaller primary particles

Primary particle diameter, generalised form:

$d_{\mathrm{pp}}[m] = k_{\mathrm{TEM}}\, d_{\mathrm{m}}{}^{D_{\mathrm{TEM}}}$ (Boies et al., 2015; Dastanpour & Rogak, 2014)

$d_{\mathrm{pp}}^3 = (k_{\mathrm{TEM}}{}^3) d_{\mathrm{m}}{}^{3D_{\mathrm{TEM}}}$

Number of primary particles,

$n_{\mathrm{pp}} = k_{\mathrm{a}} (\frac{d_{\mathrm{m}}}{d_{\mathrm{pp}}})^{2D_\alpha}$ (Boies et al., 2015; Eggersdorfer et al., 2012a)

$n_{\mathrm{pp}} = k_{\mathrm{a}} (\frac{d_{\mathrm{m}}{}^{2D_\alpha}}{k_{\mathrm{TEM}}{}^{2D_\alpha} \times d_{\mathrm{m}}{}^{2D_{\mathrm{TEM}} D_\alpha}})$ [Substitute $d_{\mathrm{pp}} = k_{\mathrm{TEM}}\, d_{\mathrm{m}}{}^{D_{\mathrm{TEM}}}$]

Mass of BC aggregate is the sum of the mass of primary particles:

Assumption: Single point of contact between pairs of primary particles, where the overlapping coefficient, $C_{ov} = 0$

$m = n_{\mathrm{pp}} \rho_0 (\frac{\pi}{6}) d_{\mathrm{pp}}{}^3$ [Substitute $n_{\mathrm{pp}} = k_{\mathrm{a}} (\frac{d_{\mathrm{m}}{}^{2D_\alpha}}{k_{\mathrm{TEM}}{}^{2D_\alpha} \times d_{\mathrm{m}}{}^{2D_{\mathrm{TEM}} D_\alpha}})$ & $d_{\mathrm{pp}}^3 = (k_{\mathrm{TEM}}{}^3) d_{\mathrm{m}}{}^{3D_{\mathrm{TEM}}}$]

$m = k_{\mathrm{a}} (\frac{d_{\mathrm{m}}{}^{2D_\alpha}}{k_{\mathrm{TEM}}{}^{2D_\alpha} \times d_{\mathrm{m}}{}^{2D_{\mathrm{TEM}} D_\alpha}}) \times \rho_0 (\frac{\pi}{6}) (k_{\mathrm{TEM}}{}^3) d_{\mathrm{m}}{}^{3D_{\mathrm{TEM}}}$

$m = k_{\mathrm{a}} d_{\mathrm{m}}{}^{2D_\alpha - 2D_{\mathrm{TEM}} D_\alpha + 3D_{\mathrm{TEM}}} \rho_0 (\frac{\pi}{6}) (k_{\mathrm{TEM}})^{3-2D_\alpha}$

$m = k_{\mathrm{a}} d_{\mathrm{m}}{}^{3D_{\mathrm{TEM}} + (1 - D_{\mathrm{TEM}})2D_\alpha} \rho_0 (\frac{\pi}{6}) (k_{\mathrm{TEM}})^{3-2D_\alpha}$

$m = k_{\mathrm{a}} d_{\mathrm{m}}{}^{\varphi} \rho_0 (\frac{\pi}{6}) (k_{\mathrm{TEM}})^{3-2D_\alpha}$ where $\varphi = 3D_{\mathrm{TEM}} + (1 - D_{\mathrm{TEM}})2D_\alpha$

Mass of a collection of aggregates with size distribution n(d_{m}):

$M = \int_0^\infty m(d_{\mathrm{m}}) n(d_{\mathrm{m}})\, dlog d_{\mathrm{m}}$ [Substitute $m(d_{\mathrm{m}}) = k_{\mathrm{a}} d_{\mathrm{m}}{}^{\varphi} \rho_0 (\frac{\pi}{6}) (k_{\mathrm{TEM}})^{3-2D_\alpha}$]

$$M = \int_0^\infty k_{\mathrm{a}} d_{\mathrm{m}}{}^{\varphi} \rho_0 (\frac{\pi}{6}) (k_{\mathrm{TEM}})^{3-2D_\alpha}\, n(d_{\mathrm{m}})\, dlog d_{\mathrm{m}}$$

$$M = k_{\mathrm{a}} \rho_0 (\frac{\pi}{6}) (k_{\mathrm{TEM}})^{3-2D_\alpha} \int_0^\infty d_{\mathrm{m}}{}^{\varphi}\, n(d_{\mathrm{m}})\, dlog d_{\mathrm{m}}$$

Note:

$n(d_{\mathrm{m}}) = N \times p(d_{\mathrm{m}})$ where $p(d_{\mathrm{m}})$ is the probability density function of distribution $n(d_{\mathrm{m}})$

$\int_{-\infty}^{\infty} p(d_{\mathrm{m}}) = 1$ integrating the total interval of a probability density function is equal to 1

$$M = k_{\mathrm{a}}\rho_0(\frac{\pi}{6})(k_{\mathrm{TEM}})^{3-2D_{\alpha}} \int_0^{\infty} d_{\mathrm{m}}{}^{\varphi}\, N\, p(d_{\mathrm{m}})\, dlogd_{\mathrm{m}}$$

$$M = N \times k_{\mathrm{a}}\rho_0(\frac{\pi}{6})(k_{\mathrm{TEM}})^{3-2D_{\alpha}} \int_0^{\infty} d_{\mathrm{m}}{}^{\varphi}\, dlogd_{\mathrm{m}}$$

Note: The remaining integral, $\int_0^{\infty} d_{\mathrm{m}}{}^{\varphi}\, dlogd_{\mathrm{m}}$ is the φ^{th} moment of a log-normal distribution

Moment Generating Function of order φ for the log-normal distribution:

$$M_{\varphi}(\mu, \sigma) = e^{\varphi\mu + \frac{\varphi^2\sigma^2}{2}}$$ (Magnus et al., 2013)

or similarly, $E(X^{\varphi}) = \exp(\varphi\mu + \frac{1}{2}\varphi^2\sigma^2)$

$$M = N\rho_0(\frac{\pi}{6})(k_{\mathrm{TEM}})^{3-2D_{\alpha}} \exp(\varphi\mu + \frac{1}{2}\varphi^2\sigma^2)$$

Note: $\mu = \ln(\mathrm{GMD})$ & $\sigma = \ln(\mathrm{GSD})$

$$M = Nk_{\mathrm{a}}\rho_0(\frac{\pi}{6})(k_{\mathrm{TEM}})^{3-2D_{\alpha}} \exp(\varphi \times \ln(\mathrm{GMD}) + \frac{1}{2}\varphi^2 \times [\ln(\mathrm{GSD})]^2)$$

Recall Logarithmic Power Rule: $log_b(x^y) = y.log_b(x)$

$$M = Nk_{\mathrm{a}}\rho_0(\frac{\pi}{6})(k_{\mathrm{TEM}})^{3-2D_{\alpha}} \exp(\ln(\mathrm{GMD}^{\varphi}) + \frac{1}{2}\varphi^2 \times [\ln(\mathrm{GSD})]^2)$$

$$M = Nk_{\mathrm{a}}\rho_0\left(\frac{\pi}{6}\right)(k_{\mathrm{TEM}})^{3-2D_{\alpha}}\, \mathrm{GMD}^{\varphi} \exp(\frac{\varphi^2 \ln(\mathrm{GSD})^2}{2})$$ where $\varphi = 3D_{\mathrm{TEM}} + (1 - D_{\mathrm{TEM}})2D_{\alpha}$

Rearranging equation for *N* – Simplified FA Model:

$$N = \frac{M}{k_{\mathrm{a}}\rho_0(\frac{\pi}{6})(k_{\mathrm{TEM}})^{3-2D_{\alpha}}\, \mathrm{GMD}^{\varphi} \exp(\frac{\varphi^2 \ln(GSD)^2}{2})}$$ where $\varphi = 3D_{\mathrm{TEM}} + (1 - D_{\mathrm{TEM}})2D_{\alpha}$

When $k_{\mathrm{a}} = 1$ and $D_{\alpha} = \frac{1}{2}D_{fm}$ is assumed for aircraft BC emissions, the FA model becomes:

$$\mathrm{EI_n} = \frac{\mathrm{EI_m}}{\rho_0(\frac{\pi}{6})(k_{\mathrm{TEM}})^{3-D_{\mathrm{fm}}}\, \mathrm{GMD}^{\varphi} \exp(\frac{\varphi^2 \ln(GSD)^2}{2})}$$ where $\varphi = 3D_{\mathrm{TEM}} + (1 - D_{\mathrm{TEM}})D_{\mathrm{fm}}$

M = Total mass of BC aggregates
N = Total number of BC aggregates
ρ_0 = Material density of BC
D_{fm} = Aggregate mass-mobility exponent
k_{a} & D_{α} = Scaling prefactor & projected area exponent
k_{TEM} & D_{TEM} = TEM prefactor-exponent coefficient pairs
GMD = Geometric mean diameter
GSD = Geometric standard deviation

Earlier derivations of the FA model can be found in Stettler & Boies (2014), Teoh et al. (2017), Stettler et al. (2017), Teoh et al. (2018a) and Teoh et al. (2018b).

S1.2 Extended Derivation of the FA Model (Eq. 16, main text) including C_{ov}

Derivation of $N = \frac{M}{\rho_0\left(\frac{\pi}{6}\right)[k_a(k_{TEM})^{3-2D_\alpha}GMD^{\varphi}\exp\left(\frac{\varphi^2\ln(GSD)^2}{2}\right)\left(1-1.5C_{ov}^2+0.5C_{ov}^3\right)+k_{TEM}^3(\frac{1}{2})(1.5C_{ov}^2-0.5C_{ov}^3)GMD^{\gamma}\exp\left(\frac{\gamma^2\ln(GSD)^2}{2}\right)]}$

where $\varphi = 3D_{TEM} + (1 - D_{TEM})2D_\alpha$ & $\gamma = 3D_{TEM}$

<u>Equations from Section S1.1</u>:

Primary particle diameter, $d_{pp}^3 = ({k_{TEM}}^3){d_m}^{3D_{TEM}}$

Number of primary particles, $n_{pp} = k_a\left(\frac{{d_m}^{2D_\alpha}}{{k_{TEM}}^{2D_\alpha} \times {d_m}^{2D_{TEM}D_\alpha}}\right)$

For monodisperse primary particles, the mass of one BC aggregate with overlapping primary particles is defined by Moran et al. (2018) as:

$$m = \rho_0\left(\frac{\pi}{6}\right){d_{pp}}^3 \times \left[n_{pp} - (n_{pp} - 1)\left(\frac{1}{2}\right)(3 - C_{ov}){C_{ov}}^2\right]$$

$$m = \rho_0\left(\frac{\pi}{6}\right)[{d_{pp}}^3 n_{pp} - {d_{pp}}^3 n_{pp}\left(\frac{1}{2}\right)(3 - C_{ov}){C_{ov}}^2 + {d_{pp}}^3(\frac{1}{2})(3 - C_{ov}){C_{ov}}^2]$$

[Substitute $n_{pp} = k_a\left(\frac{{d_m}^{2D_\alpha}}{{k_{TEM}}^{2D_\alpha} \times {d_m}^{2D_{TEM}D_\alpha}}\right)$ & $d_{pp}^3 = ({k_{TEM}}^3){d_m}^{3D_{TEM}}$]

$$m = \rho_0 k_a {d_m}^{\varphi}(\frac{\pi}{6})(k_{TEM})^{3-2D_\alpha} - \rho_0 k_a {d_m}^{\varphi}(\frac{\pi}{6})(k_{TEM})^{3-2D_\alpha}\left(\frac{1}{2}\right)(3 - C_{ov}){C_{ov}}^2 + \rho_0 {d_m}^{\gamma}(\frac{\pi}{6})(k_{TEM})^3\left(\frac{1}{2}\right)(3 - C_{ov}){C_{ov}}^2$$

where $\varphi = 3D_{TEM} + (1 - D_{TEM})2D_\alpha$, and $\gamma = 3D_{TEM}$

Mass of a collection of aggregates with size distribution n(d_m):

$$M = \int_0^\infty m(d_m)n(d_m)\, dlogd_m$$

$$M = \int_0^\infty [\rho_0 k_a {d_m}^{\varphi}(\frac{\pi}{6})(k_{TEM})^{3-2D_\alpha} - \rho_0 k_a {d_m}^{\varphi}(\frac{\pi}{6})(k_{TEM})^{3-2D_\alpha}\left(\frac{1}{2}\right)(3 - C_{ov}){C_{ov}}^2 + \rho_0 {d_m}^{\gamma}\left(\frac{\pi}{6}\right)\left(k_{TEM}\right)^3\left(\frac{1}{2}\right)(3 - C_{ov}){C_{ov}}^2\Big] \times n(d_m)\, dlogd_m$$

$$M = \rho_0(\frac{\pi}{6})k_a(k_{TEM})^{3-2D_\alpha}\int_0^\infty {d_m}^{\varphi}n(d_m)\, dlogd_m - \rho_0(\frac{\pi}{6})k_a(k_{TEM})^{3-2D_\alpha}\left(\frac{1}{2}\right)(3 - C_{ov}){C_{ov}}^2\int_0^\infty {d_m}^{\varphi}n(d_m)\, dlogd_m + \rho_0(\frac{\pi}{6})k_a(k_{TEM})^3\left(\frac{1}{2}\right)(3 - C_{ov}){C_{ov}}^2\int_0^\infty {d_m}^{\gamma}n(d_m)\, dlogd_m$$

$$M = Nk_a\rho_0(\frac{\pi}{6})(k_{TEM})^{3-2D_\alpha}GMD^{\phi}\exp\left(\frac{\phi^2\ln(GSD)^2}{2}\right) - Nk_a\rho_0(\frac{\pi}{6})(k_{TEM})^{3-2D_\alpha}\left(\frac{1}{2}\right)(3 - C_{ov}){C_{ov}}^2 GMD^{\phi}\exp\left(\frac{\phi^2\ln(GSD)^2}{2}\right) + Nk_a\rho_0(\frac{\pi}{6})(k_{TEM})^3\left(\frac{1}{2}\right)(3 - C_{ov}){C_{ov}}^2 GMD^{\gamma}\exp(\frac{\gamma^2\ln(GSD)^2}{2})$$

Rearranging equation for *N* – Extended FA Model:

$$N = \frac{M}{\rho_0\left(\frac{\pi}{6}\right)[k_a(k_{TEM})^{3-2D_\alpha}GMD^{\varphi}\exp\left(\frac{\varphi^2\ln(GSD)^2}{2}\right)\left(1-1.5C_{ov}^2+0.5C_{ov}^3\right)+k_{TEM}^3(\frac{1}{2})(1.5C_{ov}^2-0.5C_{ov}^3)GMD^{\gamma}\exp\left(\frac{\gamma^2\ln(GSD)^2}{2}\right)]}$$

where $\varphi = 3D_{TEM} + (1 - D_{TEM})2D_\alpha$, and $\gamma = 3D_{TEM}$

<u>Checks</u>: If $C_{ov} = 0$, the FA model becomes $N = \frac{M}{k_a\rho_0(\frac{\pi}{6})(k_{TEM})^{3-2D_\alpha}GMD^{\varphi}\exp(\frac{\varphi^2\ln(GSD)^2}{2})}$

S1.3 Sensitivity of the FA Model Outputs to C_{ov}

The degree of primary particle overlapping is defined as $C_{ov} = \frac{(r_i+r_j)-d_{ij}}{(r_i+r_j)}$, and C_{ov} is usually obtained from the projected overlapping coefficient estimated from TEM images ($C_{ov,p}$). Brasil et al. (1999) showed that $C_{ov,p}$ can be converted to C_{ov} with the following formula:

$$C_{ov} = \zeta_1 C_{ov,p} - \zeta_2, \qquad \text{where } \zeta_1 = 1.1 \pm 0.1 \text{ and } \zeta_2 = 0.2 \pm 0.02$$

According to Bourrous et al. (2018), the $C_{ov,p}$ for BC is between 0.2 and 0.4, and the conversion from $C_{ov,p}$ to C_{ov} gives a range of $0.02 \leq C_{ov} \leq 0.24$.

Using the SAMPLE III.2 aircraft emissions data from Boies et al. (2015), we explored the sensitivity of the FA model outputs (the estimated *N* or EI_n) to the range of C_{ov} provided by Bourrous et al. (2018). For an upper bound of C_{ov} = 0.24, Figure S2 shows that the FA model outputs could increase by up to 7% relative to the simplified FA model where C_{ov} is assumed to be 0.

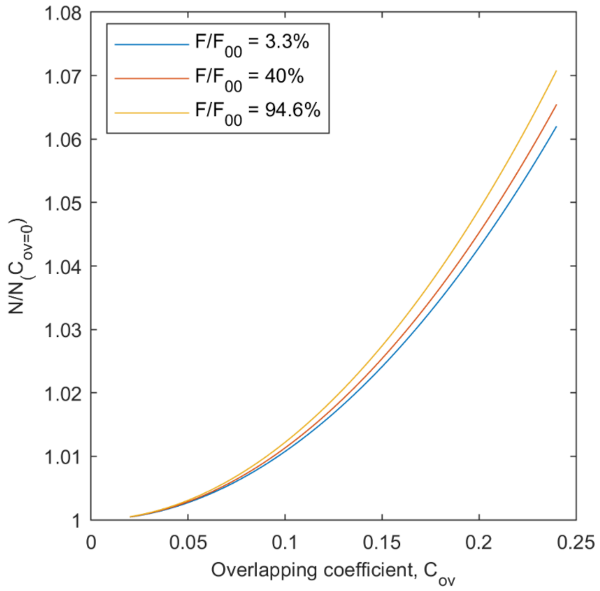

Figure S2: Sensitivity of the FA model outputs to C_{ov}, using data from the SAMPLE III.2 campaign.

S2 – ASSUMPTION OF k_a = 1 AND D_{fm} = $2D_\alpha$ FOR AIRCRAFT BC EMISSIONS

The prefactor-exponent assumptions of k_a = 1 and $2D_\alpha = D_{fm}$ are used to estimate aircraft BC emissions in the FA model. In this section, the validity of these assumptions is evaluated using different methodologies and datasets published in the literature.

For aggregates formed via diffusion limited cluster aggregation (DLCA), Eggersdorfer & Pratsinis (2012) showed that the k_a is inversely correlated with the GSD of primary particle diameters (figure 4 on Eggersdorfer & Pratsinis (2012)). Using data on the size distribution of primary particle diameters (d_{pp}) from a CFM56-7B26 single annular combustor (SAC) aircraft gas turbine engine (Liati et al., 2014), the GSD of aircraft BC primary particles at different engine thrust settings (F/F_{00}) can be estimated. This aircraft primary particle GSD can subsequently be used to estimate the range of k_a values by interpolating the results presented in figure 4 on Eggersdorfer & Pratsinis (2012).

Table S1 shows the soot primary particle size distribution data from Liati et al. (2014), while Table S2 shows the aircraft BC primary particle GMD and GSD at different F/F_{00} (which were estimated from the size distribution of BC primary particles).

Table S1: Aircraft BC primary particle size distribution data from Liati et al. (2014)

BC Primary Particle Diameter (nm)	**Mean diameter, d_i (nm)**	**Frequency (%)**		
		F/F_{00} = 0.07	**F/F_{00} = 0.65**	**F/F_{00} = 1.00**
0 – 5	2.5	0	0	2
5 – 10	7.5	10	4.5	6
10 – 15	12.5	61	17.6	16.7
15 – 20	17.5	28	32.2	24
20 – 25	22.5	1	26.7	19.3
25 – 30	27.5	0	16	15.3
30 – 35	32.5	0	2.2	8.4
35 – 40	37.5	0	0.8	4.2
40 – 45	42.5	0	0	1.8
> 45	50	0	0	2.3

The GMD and GSD of aircraft BC primary particles are estimated using the following equations (Eq. S1 and S2) from Hinds (1999):

$$\mathrm{GMD} = \exp\left(\frac{\sum_{i=1}^{j} N_i\, ln(d_m)_i}{N}\right), \qquad \text{(S1)}$$

$$\mathrm{GSD} = \exp\left(\frac{\sum_{i=1}^{j} N_i (ln(d_m)_i - ln(\mathrm{GMD}))^2}{N-1}\right)^{\frac{1}{2}}. \qquad \text{(S2)}$$

Table S2: Aircraft BC primary particle GMD and GSD at different F/F_{00}

F/F_{00}	**Primary Particle GMD (nm)**	**Primary Particle GSD**
0.07	13.1	1.2761
0.65	18.6	1.3978
1.00	19.3	1.6827

Using the aircraft primary particle GSD results from Table S2, the range of k_a is interpolated using the results presented in figure 4 on Eggersdorfer & Pratsinis (2012), adopting a DLCA assumption. For $0.07 \leq \frac{F}{F_{00}} \leq 1.0$, the interpolated k_a is within the range of 0.8 to 1.0. Hence, the assumption of k_a = 1 for aircraft BC emissions across all engine type and thrust settings is supported.

Secondly, using data from the SAMPLE III.2 campaign, k_a and D_α values at certain F/F$_{00}$ can also be approximated using Eq. S3, which is derived by equating n_{pp} from Eq. 1 and Eq. 6 in the main text, and subsequently substituting m with Eq. 2:

$$k_a = \frac{k}{\rho_0}(k_{TEM})^{2D_\alpha - 3} \quad \text{and} \quad D_\alpha = \frac{3D_{TEM} - D_{fm}}{2(D_{TEM} - 1)}. \tag{S3}$$

The variables k, D_{fm}, k_{TEM} and D_{TEM} required to estimate k_a and D_α at certain F/F$_{00}$ are available from Boies et al. (2015) and Johnson et al. (2015), where the data used in these two studies were collected from the same campaign and experimental set up. Table S3 shows the approximation of k_a and D_α values from a CFM56-5B4-2P double annular combustor (DAC) engine at certain F/F$_{00}$. Outliers from three data points (F/F$_{00}$ = 9.5% and F/F$_{00}$ = 30.9%) are identified from Johnson et al. (2015) and excluded in this analysis.

Table S3: Estimation of k_a and D_α values from a CFM56-5B4-2P DAC engine using Eq. S3.

F/F$_{00}$ - %	Boies et al. (2015)		Johnson et al. (2015)		k_{TEM} [m]	Est. D_α	Est. k_a	% difference between D_{fm} and $2D_\alpha$
	k_{TEM} [nm]	D_{TEM}	k	D_{fm}				
9.5	0.54	0.86	141.54	2.91	0.03			
17.4	0.86	0.75	7.72	2.73	0.005	0.96	1.382	-29.67%
17.4	1.39	0.65	11.72	2.76	0.001	1.157	0.764	-16.16%
17.6	0.71	0.8	32.19	2.82	0.011	1.05	1.032	-25.53%
24.4	1.17	0.74	10.28	2.75	0.005	1.019	0.888	-25.89%
24.4	0.8	0.79	33.73	2.81	0.01	1.048	1.196	-25.41%
30.9	0.44	0.98	823.33	3	0.291			
30.9	0.56	0.92	823.33	3	0.107			
					Average	**1.0468**	**1.0524**	**-24.53%**

Using this approach, the average k_a value for a DAC engine is estimated to be 1.05 ($0.75 \leq k_a \leq 1.4$), which also supports the assumption of k_a = 1 for aircraft emissions in the FA model. Finally, Table S3 also showed that values of $2D_\alpha$ and D_{fm} differs by approximately 25%, where the discrepancy could be due to the uncertainties from experimental measurements.

S3 – DETAILED METHODOLOGY & EXPERIMENTAL SET-UP OF THE DATASETS USED TO VALIDATE THE FA MODEL

This section describes the experimental set-up and methodology of the different datasets used to validate the FA Model. The FA model is validated with BC emissions data from three different sources: A compression ignition direct injection (CIDI) internal combustion engine, a soot generator, and two aircraft gas turbine engines at ground and cruise conditions.

S3.1 Validation – CIDI Internal Combustion Engine

BC emissions and aggregate morphology data from a CIDI engine, a six-cylinder Cummins ISX were obtained by Graves et al. (2015). The dataset consists of 16 data points measured from six different engine operating conditions, where the engine is set at a certain percentage of its maximum load based on the European Stationary Cycle (EU, 1999). Figure S3 shows the experimental set-up used to collect the BC emissions data from the CIDI engine.

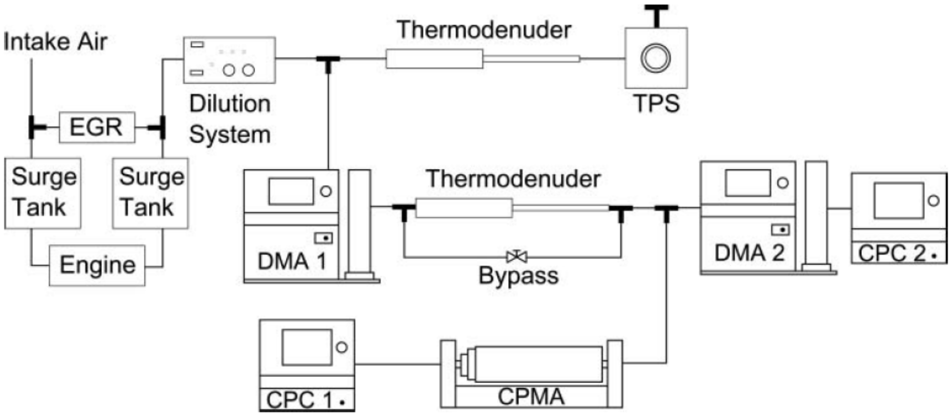

Figure S3: Experimental set-up used to collect data on the BC concentration and properties from the CIDI internal combustion engine (Graves et al. (2015), reproduced with permission).

The exhaust gas sample from the engine is first diluted at a ratio of 11:1 before passing through a differential mobility analyser (DMA; Model 3081, TSI Inc., Shoreview, MN, USA) and a thermodenuder (operating at 200°C to remove volatile particles in the sample flow). Next, the sample flow is split into two. Half of the flow passes through a second DMA and a condensation particle counter (CPC; TSI Model 3775, 5 nm D_{50}) to measure the particle number concentration for a given d_m interval (n_i). The subscript 'i' accounts for each particle size interval consisting of a defined d_m interval. The process of measuring n_i is repeated for successive particle size intervals until the entire size range is covered. Using the formulation of Gormley & Kennedy (1948), particle line loss correction factors are applied to the measured n_i to account for diffusional deposition losses along the thermodenuder. Particle losses along the sampling line and thermophoretic losses along the thermodenuder were not corrected due to the large degree of uncertainty in its correction factor (Graves et al., 2015). The total BC particle number concentration, N is calculated by the summation of n_i for each d_m interval,

$$N = \sum_{i=1}^{j} n_i \,, \qquad \text{(S3)}$$

where the subscript 'j' is the total number of size intervals covering the entire size range. For each engine operating mode, the GMD and GSD are estimated using Eq. S1 and Eq. S2.

The other half of the sample flow is sent to a CPMA to measure the average mass of one BC aggregate (m) for a given d_m interval. With measurements of m and d_m, prefactor-exponent coefficient pairs of C and D_{fm} can be estimated by a power-law fit using Eq. 2 (main text) and Eq.5 (main text) is then applied to estimate ρ_{eff}. While tandem measurements of the total BC mass concentration (M) were not directly measured in this experimental campaign, it is estimated using the integrated particle size distribution (IPSD) method (Liu et al., 2009),

$$M = \sum_{i=1}^{j} n_i (\rho_{\mathrm{eff}})_i (\frac{\pi}{6} {d_{\mathrm{m}}}^3)_i \ , \qquad \text{(S4)}$$

where the central d_m value in each size interval is used to estimate ρ_{eff} (from Eq. 7 in the main text) and the volume of BC aggregate ($\frac{\pi}{6} {d_{\mathrm{m}}}^3$). Given the lack of repeated measurements for M to obtain a standard deviation, the uncertainty bound of ρ_{eff} for each engine mode was approximated from a generalised trendline ($\rho_{\mathrm{eff}} = k {d_{\mathrm{m}}}^{D_{\mathrm{fm}}-3}$) to cover 95% of the measured data points, where k and D_{fm} are extracted from Graves et al. (2015). The uncertainty bounds of ρ_{eff} are shown in Figure S4, and we assume that the uncertainties in directly propagates to the estimated M, given that m and ρ_{eff} are directly proportional, $m = \rho_{\mathrm{eff}} (\frac{\pi}{6}) {d_{\mathrm{m}}}^3$.

Using the same CIDI engine, Dastanpour et al. (2016) found k_a and D_α values for each engine operating mode, which will be referred to as $k_{a,opt}$ and $D_{\alpha,opt}$. Values of $k_{a,opt}$ and $D_{\alpha,opt}$ (presented in Table S4) are estimated using a least squares regression between TEM determined d_{pp} and Eq. S5 (Dastanpour et al., 2016), which is derived by equating Eq. 1 and Eq. 8 in the main text,

$$d_{pp} = \left(\frac{\pi k_a \rho_0}{6m} (d_m)^{2D_\alpha} \right)^{\frac{1}{2D_\alpha - 3}}, \qquad \text{(S5)}$$

The performance of the FA model is compared by using (i) $k_{a,opt}$ and $D_{\alpha,opt}$ values from Dastanpour et al. (2016), and (ii) the constant $k_a = 0.998$ and $D_\alpha = 1.069$ values (Eggersdorfer et al., 2012b) in Section 4.1 (main text). Finally, k_{TEM} and D_{TEM} coefficients of 2.644×10^{-6} and 0.39 are used for all engine modes (Dastanpour & Rogak, 2014).

Table S4: Fitted values of $k_{a,opt}$ and $D_{\alpha,opt}$ for each engine mode from Table 2 of Dastanpour et al. (2016)

Engine Mode	$D_{\alpha,opt}$	$k_{a,opt}$
B75 20% EGR	1.08	0.83
B75 0% EGR	1.2	0.79
B50 20% EGR	1.13	1.13
B37 20% EGR	1.13	1.2
B25 20% EGR	1.01	1.4
A63 80% Premixed	1.1	1.19

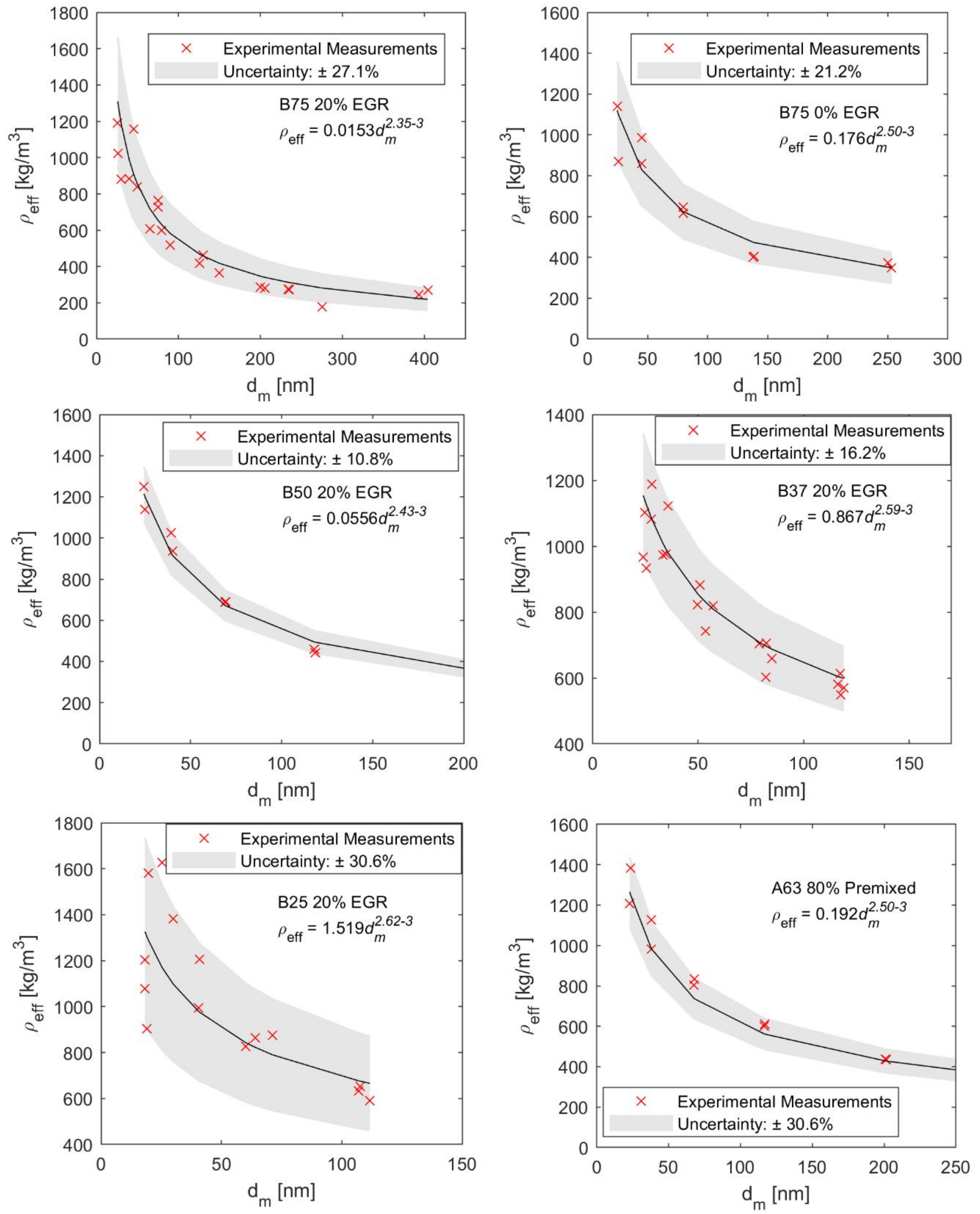

Figure S4: Uncertainty bounds of ρ_{eff} for each engine mode of the CIDI engine, which are then propagated to estimate the uncertainties of *M*. Values of *k* and D_{fm} are obtained from Graves et al. (2015).

S3.2 Validation – Soot Generator

A laboratory-based experiment was conducted at the combustion laboratory in the University of Cambridge to measure the emissions characteristic of BC produced by a soot generator. The custom-made soot generator was previously used by Stettler et al. (2013b) to evaluate the dependence of smoke number (SN) and mass concentration of BC (C_{BC}) on the BC particle size distribution. Figure S5 shows the schematic diagram of the experimental set-up.

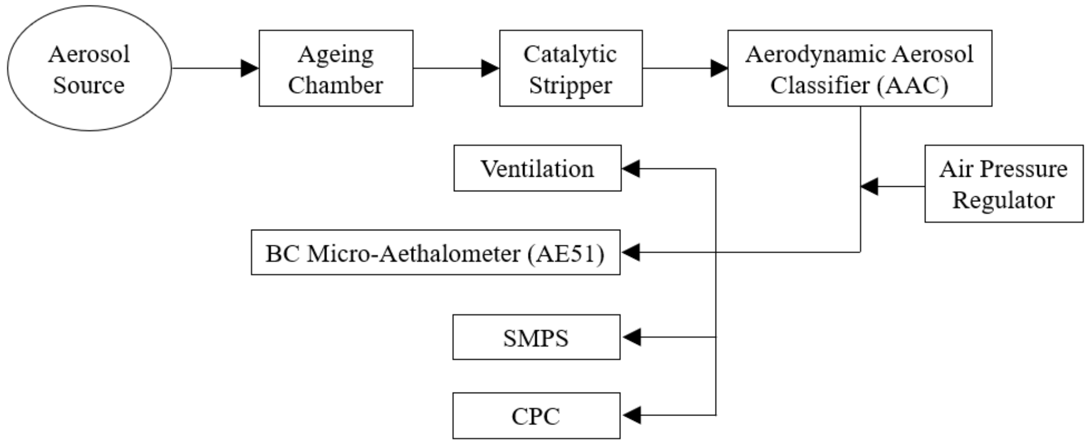

Figure S5: Experimental set-up to measure the BC concentration and properties produced from a soot generator.

BC aggregates are produced from a burner/soot generator by mixing propane (C_3H_8), nitrogen (N_2), and air in a co-flow inverse diffusion flame, and sampled at around 200mm above the flame by a stainless-steel probe. The sample flow then enters an ageing chamber to coagulate and form larger BC aggregates with steady sizes, and the BC concentration and size distribution are varied by changing the residence time in the ageing chamber. A catalytic stripper with an internal temperature setting of 350°C is then connected downstream to remove volatile particles. Stainless steel and conductive silicone tubing are used to minimise the particle losses along the sampling flow, and no particle line loss corrections were applied.

Following the catalytic stripper, the aerodynamic aerosol classifier (AAC, Cambustion, United Kingdom) is set to select four particle sizes, which were 50nm, 100nm, 150nm and 200nm respectively to obtain BC particles that are monodisperse. The particle size distribution is measured using a scanning mobility particle sizer (SMPS, TSI, Inc., Shoreview, MN, USA:3080 Electrostatic Classifier, 3081 DMA, 3776 condensation particle counter [CPC]), of which diffusion and multiple charge correction have been applied. Simultaneously, repeated measurements of *N* and *M* are made by a CPC and Micro-Aethalometer (MicroAeth AE51, AethLabs, United States) respectively.

Overall, 13 data points are produced from this experiment and their corresponding particle size distributions are shown in Figure S6. Although particle line loss correction factors were not applied, stainless steel and conductive silicon tubing were both used to minimise the particle losses along the sampling flow.

The assumed k_{TEM} and D_{TEM} coefficients are 2.465×10^{-6} and 0.29 respectively (Dastanpour & Rogak, 2014), while constant values of k_a = 0.998 and D_α = 1.069 (Eggersdorfer et al., 2012b) were used due to the lack of data on the $k_{a,opt}$ and $D_{\alpha,opt}$ values.

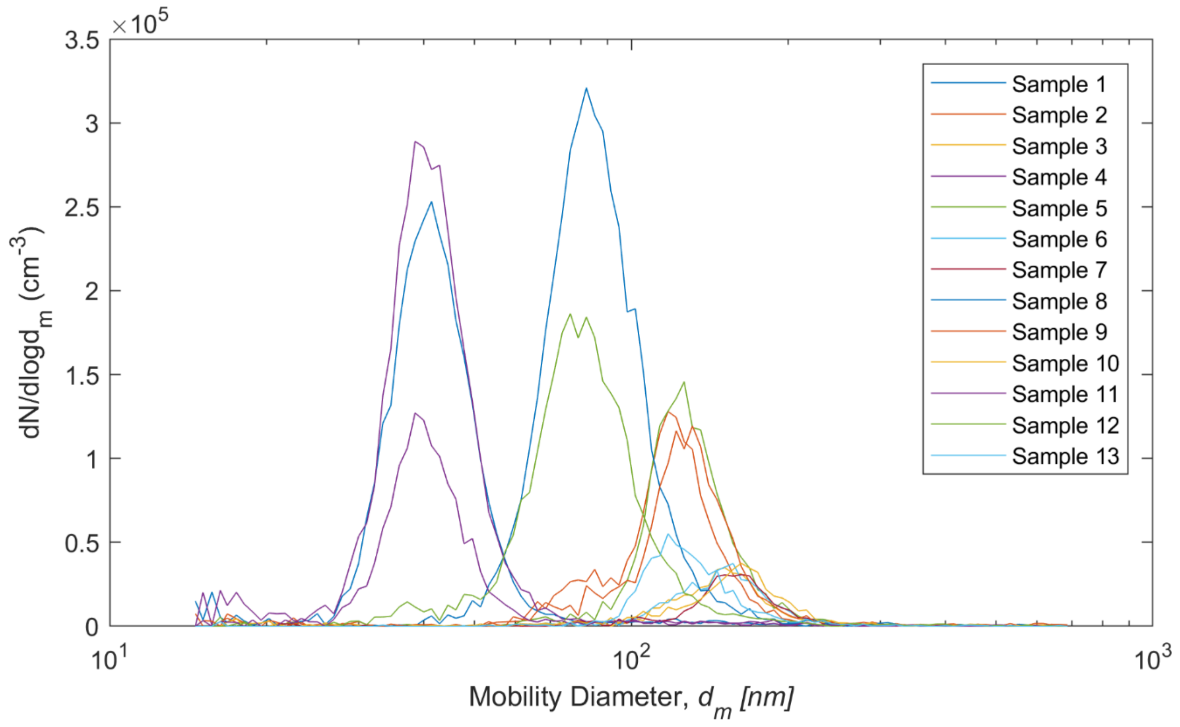

Figure S6: BC particle size distribution for the 13 data points produced by the soot generator.

S3.3 Additional Notes for Validation of Aircraft Gas Turbine Engines

Ground-level BC measurements from other studies (Lobo et al., 2015; Timko et al., 2010; Wey et al., 2006) were not included due to a lack of volatile particle remover (VPR) that could have led to the inclusion of some volatile particles. Additionally, an SMPS cut-off size of 15 nm could also lead to an underestimation of EI_n at lower engine thrust settings (< 7% F/F_{00}), where aircraft BC d_m is estimated to be below 15 nm (Durdina et al., 2014).

S4 – FA MODEL VALIDATION FOR THE CIDI ENGINE

The respective $k_{a,opt}$ and $D_{\alpha,opt}$ values for each engine mode are previously listed in Table S4, while $k_{TEM} = 2.64\text{x}10^{-6}$ and $D_{TEM} = 0.29$ is prescribed for all engine operating conditions (Dastanpour & Rogak, 2014). The validation data used in Figure 1a (main text) is presented in Table S5.

Additionally, the same CIDI dataset is also validated by using constant values of $k_a = 0.998$ and $D_\alpha = 1.069$ (Eggersdorfer et al., 2012b), of which results were presented in Figure S7 and Table S6. The R^2 value remains high at 0.978 but the magnitude of normalised mean bias (NMB) increased slightly from -8.3% ($k_{a,opt}$ and $D_{\alpha,opt}$) to +15.5% ($k_a = 0.998$ and $D_\alpha =$ 1.069). This shows that the constant k_a and D_α values from Eggersdorfer et al. (2012b) can be used when $k_{a,opt}$ and $D_{\alpha,opt}$ data are unavailable.

Table S5: Validation data for the CIDI engine (Figure 1a in the main text), where $k_{a,opt}$ and $D_{\alpha,opt}$ values are used.

Measured Values						Estimated Values - FA Model			
Engine Mode	M (kg/m^3)	GMD (nm)	GSD	N (m^{-3})	φ	N (m^{-3})	(yi-ŷi)²	(yi-ȳ)²	NMB
B75 20% EGR	1.80E-05	90.01	1.573	4.44E+13	2.404	5.72E+13	1.6E+26	8.2E+26	21.40%
	1.46E-05	86.55	1.576	3.99E+13	2.404	5.06E+13	1.2E+26	5.7E+26	19.67%
	1.37E-05	84.69	1.58	4.55E+13	2.404	5.00E+13	2.0E+25	8.8E+26	3.55%
B75 0% EGR	3.52E-06	63.07	1.555	2.12E+13	2.574	1.99E+13	1.5E+24	2.8E+25	-9.69%
	3.58E-06	65.72	1.539	2.10E+13	2.574	1.88E+13	4.9E+24	2.6E+25	-14.27%
B50 20% EGR	2.42E-06	58.02	1.558	1.64E+13	2.475	1.44E+13	3.8E+24	2.3E+23	-16.36%
	2.24E-06	56.97	1.562	1.78E+13	2.475	1.39E+13	1.6E+25	3.8E+24	-26.03%
B37 20% EGR	2.68E-07	36.66	1.564	5.77E+12	2.475	4.64E+12	1.3E+24	1.0E+26	-23.59%
	1.26E-06	47.91	1.545	1.37E+13	2.475	1.16E+13	4.4E+24	4.7E+24	-19.61%
	5.07E-07	39.5	1.567	8.57E+12	2.475	7.26E+12	1.7E+24	5.4E+25	-19.60%
	3.32E-07	38.26	1.601	6.38E+12	2.475	4.84E+12	2.4E+24	9.0E+25	-28.01%
B25 20% EGR	1.03E-07	31.38	1.801	1.93E+12	2.304	1.93E+12	2.3E+19	2.0E+26	-6.41%
	9.96E-08	30.31	1.828	1.80E+12	2.304	1.93E+12	1.7E+22	2.0E+26	0.21%
	1.26E-07	30.56	1.827	2.28E+12	2.304	2.39E+12	1.4E+22	1.9E+26	-1.79%
A63 80% Premixed	1.07E-06	62.8	1.798	3.63E+12	2.432	3.53E+12	1.1E+22	1.5E+26	-8.15%
	1.17E-06	62.36	1.777	4.02E+12	2.432	4.06E+12	1.9E+21	1.4E+26	-4.43%
						$\sum$	3.3E+26	3.4E+27	$\overline{\text{NMB}} = -8.32\%$
						R^2	0.903		

Table S6: Validation data for the CIDI engine, where constant k_a = 0.998 and D_α =1.069 values from Eggersdorfer et al. (2012b) are used.

Measured Values						Estimated Values - FA Model			
Engine Mode	M (kg/m^3)	GMD (nm)	GSD	N (m^{-3})	φ	N (m^{-3})	(yi-ŷi)²	(yi-ȳ)²	NMB
B75 20% EGR	1.80E-05	90.01	1.573	4.44E+13	2.388	4.95E+13	2.5E+25	8.2E+26	11.28%
	1.46E-05	86.55	1.576	3.99E+13	2.388	4.37E+13	1.5E+25	5.7E+26	9.63%
	1.37E-05	84.69	1.58	4.55E+13	2.388	4.32E+13	5.5E+24	8.8E+26	-5.16%
B75 0% EGR	3.52E-06	63.07	1.555	2.12E+13	2.388	2.33E+13	4.5E+24	2.8E+25	10.04%
	3.58E-06	65.72	1.539	2.10E+13	2.388	2.20E+13	1.0E+24	2.6E+25	4.82%
B50 20% EGR	2.42E-06	58.02	1.558	1.64E+13	2.388	1.94E+13	9.3E+24	2.3E+23	18.64%
	2.24E-06	56.97	1.562	1.78E+13	2.388	1.87E+13	7.4E+23	3.8E+24	4.81%
B37 20% EGR	2.68E-07	36.66	1.564	5.77E+12	2.388	6.39E+12	3.8E+23	1.0E+26	10.70%
	1.26E-06	47.91	1.545	1.37E+13	2.388	1.63E+13	6.7E+24	4.7E+24	18.92%
	5.07E-07	39.5	1.567	8.57E+12	2.388	1.01E+13	2.2E+24	5.4E+25	17.27%
	3.32E-07	38.26	1.601	6.38E+12	2.388	6.71E+12	1.1E+23	9.0E+25	5.15%
B25 20% EGR	1.03E-07	31.38	1.801	1.93E+12	2.388	2.35E+12	1.8E+23	2.0E+26	21.73%
	9.96E-08	30.31	1.828	1.80E+12	2.388	2.34E+12	3.0E+23	2.0E+26	30.26%
	1.26E-07	30.56	1.827	2.28E+12	2.388	2.90E+12	3.9E+23	1.9E+26	27.59%
A63 80% Premixed	1.07E-06	62.8	1.798	3.63E+12	2.388	4.68E+12	1.1E+24	1.5E+26	28.94%
	1.17E-06	62.36	1.777	4.02E+12	2.388	5.38E+12	1.9E+24	1.4E+26	33.93%
						$\sum$	7.4E+25	3.4E+27	$\overline{\text{NMB}} = 15.53\%$
						R^2	0.978		

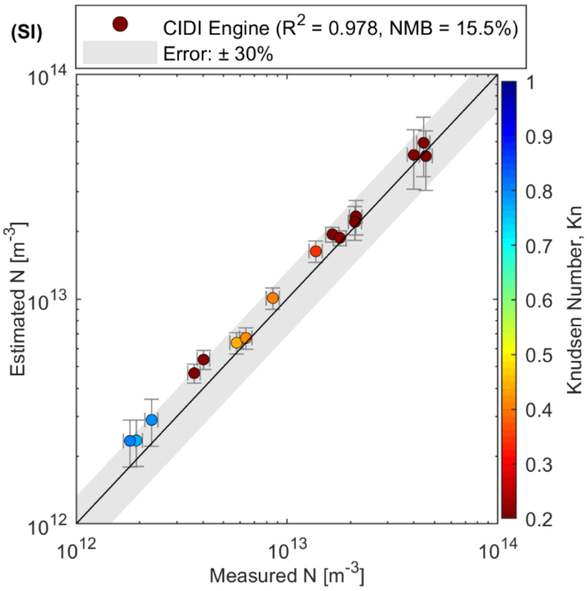

Figure S7: Validation of the FA model against emissions from a CIDI engine where constant values of k_a = 0.998 and D_α = 1.069 are used. Error bars denote precision errors from repeated measurements with 1.96σ and do not include systematic uncertainties arising from instrumentations. Detailed data tables in Table S6.

S5 – FA MODEL VALIDATION FOR THE SOOT GENERATOR

For this validation, constant values of k_a = 0.998 and D_α = 1.069 (Eggersdorfer et al., 2012b) were used due to the lack of data on the $k_{a,opt}$ and $D_{\alpha,opt}$ values. The validation data used in Figure 1b (main text) is presented in Table S7.

Table S7: Validation data for the soot generator (Figure 1b in the main text), constant values of k_a = 0.998 and D_α = 1.069 (Eggersdorfer et al., 2012b) were used.

Measured Values						Estimated Values - FA Model			
Sample	***M*** **(μg/m³)**	N_{CPC} **(m^{-3})**	**GMD (nm)**	**GSD**	**φ**	***N*** **(m^{-3})**	**$(y_i-\hat{y}_i)^2$**	**$(y_i-\bar{y})^2$**	**NMB**
1	0.768	5.37E+10	41.62	1.338	2.388	1.88E+10	1.2E+21	9.2E+20	-65.1%
2	8.187	1.97E+10	111.92	1.479	2.388	1.55E+10	1.8E+19	1.3E+19	-21.4%
3	4.099	5.23E+09	128.78	1.801	2.388	3.21E+09	4.1E+18	3.3E+20	-38.7%
4	0.726	3.83E+10	40.73	1.350	2.388	1.84E+10	4.0E+20	2.2E+20	-51.9%
5	10.250	2.03E+10	124.62	1.346	2.388	1.81E+10	5.1E+18	9.4E+18	-11.1%
6	4.561	4.79E+09	147.08	1.271	2.388	5.91E+09	1.3E+18	3.5E+20	23.5%
7	4.561	4.79E+09	143.35	1.580	2.388	4.08E+09	5.0E+17	3.5E+20	-14.8%
8	8.331	5.76E+10	85.42	1.279	2.388	3.92E+10	3.4E+20	1.2E+21	-31.9%
9	9.799	1.85E+10	120.43	1.499	2.388	1.51E+10	1.1E+19	2.4E+19	-18.1%
10	5.825	5.69E+09	145.40	1.579	2.388	5.04E+09	4.1E+17	3.1E+20	-11.3%
11	0.380	1.69E+10	42.39	1.418	2.388	8.00E+09	7.9E+19	4.2E+19	-52.7%
12	4.228	3.67E+10	80.31	1.354	2.388	2.11E+10	2.4E+20	1.8E+20	-42.5%
13	3.994	9.15E+09	127.69	1.313	2.388	6.92E+09	5.0E+18	2.0E+20	-24.5%
						∑	2.3E+21	4.1E+21	$\overline{NMB} = -27.72\%$
							R^2	0.44	

S6 – FA MODEL VALIDATION FOR AIRCRAFT GAS TURBINE ENGINES (GROUND & CRUISE)

S6.1 Data Tables for the FA Model Validation – Aircraft Emissions

Ground validation for the aircraft gas turbine engine in Figure 2a (main text) originates from the SAMPLE III.2 experimental campaign and the data is presented in Table S8. For aircraft emissions, we assume that $k_a = 1$ and $D_\alpha = \frac{1}{2} D_{\mathrm{fm}}$ (Eggersdorfer et al., 2012b) due to a lack of data on the variation of k_a and D_α values across F/F_{00}, while values of $k_{\mathrm{TEM}} = 1.621 \times 10^{-5}$ and $D_{\mathrm{TEM}} = 0.39$ from Dastanpour & Rogak (2014) are used.

Table S8: Validation data for the aircraft gas turbine on the ground (Figure 2a in the main text), of which the data is originated from the SAMPLE III.2 experimental campaign (Boies et al., 2015).

Measured Values					Estimated Values - FA Model				
F/F_{00} - %	EI_n (kg^{-1})	EI_m (mg/kg)	GMD (nm)	GSD	φ	EI_n (kg^{-1})	$(y_i-\hat{y}_i)^2$	$(y_i-\bar{y})^2$	NMB
3.32%	1.27E+15	25.1	16.09	1.76	2.854	1.79E+15	9.51E+28	6.75E+27	-24.27%
3.30%	1.22E+15	13.5	15.89	1.78	2.854	9.66E+14	5.36E+28	1.79E+28	-18.99%
3.30%	1.23E+15	13.6	15.88	1.77	2.854	9.91E+14	6.26E+28	1.55E+28	-20.38%
3.31%	1.25E+15	13.3	15.90	1.76	2.854	9.81E+14	8.63E+28	1.05E+28	-23.49%
3.30%	1.21E+15	12.9	15.96	1.76	2.854	9.60E+14	2.31E+28	1.98E+28	-12.54%
3.31%	1.20E+15	14.1	15.97	1.75	2.854	1.06E+15	1.33E+28	2.26E+28	-9.60%
3.32%	1.19E+15	14.1	15.93	1.74	2.854	1.09E+15	8.12E+28	2.66E+28	-23.96%
3.31%	1.87E+15	12.0	15.94	1.75	2.854	9.08E+14	3.10E+29	2.69E+29	-29.74%
7.62%	2.44E+15	37.2	21.16	1.73	2.854	1.32E+15	4.66E+29	1.17E+30	-28.05%
9.37%	3.11E+15	63.1	23.25	1.72	2.854	1.76E+15	6.16E+29	3.07E+30	-25.28%
11.20%	3.35E+15	108.5	25.77	1.71	2.854	2.33E+15	5.56E+29	3.98E+30	-22.28%
13.29%	3.65E+15	138.9	27.28	1.70	2.854	2.62E+15	3.96E+29	5.30E+30	-17.21%
15.50%	3.33E+15	192.3	29.23	1.69	2.854	3.05E+15	3.81E+27	3.92E+30	1.85%
17.70%	4.19E+15	262.9	33.52	1.61	2.854	3.42E+15	2.30E+27	8.07E+30	-1.14%
20.51%	4.71E+15	385.3	35.02	1.63	2.854	4.17E+15	2.02E+27	1.13E+31	0.95%
23.33%	2.20E+14	519.6	37.45	1.62	2.854	4.79E+15	3.54E+27	1.28E+30	27.03%
26.39%	2.20E+14	7.8	20.59	1.76	2.854	2.81E+14	9.03E+25	1.28E+30	4.32%
33.06%	1.87E+14	5.6	19.58	1.76	2.854	2.31E+14	3.25E+26	1.36E+30	9.63%
36.87%	1.14E+14	5.2	19.89	1.76	2.854	2.06E+14	7.62E+26	1.53E+30	24.15%
41.12%	8.85E+13	2.7	18.49	1.73	2.854	1.43E+14	7.68E+26	1.60E+30	31.30%
45.75%	6.91E+13	2.2	18.58	1.73	2.854	1.17E+14	1.53E+27	1.65E+30	56.70%
51.09%	5.34E+13	2.2	18.85	1.73	2.854	1.09E+14	9.81E+26	1.69E+30	58.66%
57.10%	4.16E+13	1.8	19.17	1.73	2.854	8.51E+13	9.15E+26	1.72E+30	72.78%
62.91%	3.36E+13	1.7	19.74	1.73	2.854	7.21E+13	6.11E+26	1.74E+30	73.51%
69.13%	1.52E+13	1.6	20.73	1.74	2.854	5.86E+13	4.71E+26	1.79E+30	142.57%
85.70%	6.19E+12	1.3	22.75	1.73	2.854	3.71E+13	1.36E+27	1.81E+30	595.22%
94.60%	1.44E+13	1.4	22.90	1.70	2.854	4.32E+13	4.01E+26	1.79E+30	139.27%
84.33%	6.32E+14	1.2	23.00	1.71	2.854	3.46E+13	4.53E+27	5.20E+29	10.65%
3.32%	1.04E+15	9.4	16.26	1.74	2.854	7.01E+14	2.76E+28	9.69E+28	-15.95%
3.38%	1.69E+15	12.6	16.44	1.75	2.854	8.78E+14	2.35E+29	1.11E+29	-28.74%
6.55%	2.86E+15	31.7	20.81	1.72	2.854	1.21E+15	2.82E+29	2.27E+30	-18.55%
9.75%	3.50E+15	66.0	24.34	1.71	2.854	1.67E+15	1.87E+28	4.63E+30	3.90%
13.25%	2.10E+14	125.0	27.50	1.69	2.854	2.34E+15	5.66E+26	1.31E+30	11.35%
20.52%	9.12E+14	327.0	34.70	1.63	2.854	3.67E+15	1.64E+28	1.94E+29	-14.06%
26.45%	2.09E+14	5.5	19.46	1.75	2.854	2.35E+14	1.91E+25	1.31E+30	2.09%
3.44%	1.27E+15	12.1	17.30	1.72	2.854	7.86E+14	9.51E+28	6.75E+27	-24.27%
26.78%	1.22E+15	5.3	19.49	1.77	2.854	2.15E+14	5.36E+28	1.79E+28	-18.99%
						∑	3.36E+30	6.69E+31	$\overline{NMB}$ = 26.6%
						R^2	0.950		

Next, cruise validation for the aircraft gas turbine engine in Figure 2b (main text) originates from the NASA ACCESS experimental campaign and the data is presented in Table S9. Two observed GSD values in red (on the table above) have been highlighted due to the potential of an anomaly or measurement error.

Table S9: Validation data for the aircraft gas turbine at cruise conditions (Figure 2b in the main text), of which the data is originated from the NASA ACCESS experimental campaign (Moore et al., 2017).

Measured Values						Estimated Values - FA Model			
Fuel Type	**EI_n (kg^{-1})**	**EI_m (mg/kg)**	**GMD (nm)**	**GSD (nm)**	**φ**	**EI_n (kg^{-1})**	**$(y_i-\hat{y}_i)^2$**	**$(y_i-\bar{y})^2$**	**NMB**
Conventional	7.64E+14	80.97	35.3	1.72	2.76	6.85E+14	6.32E+27	1.30E+29	-10.40%
Conventional	5.00E+14	39.58	29.7	1.64	2.76	6.70E+14	2.88E+28	9.30E+27	33.95%
Conventional	4.50E+14	32.26	25.5	1.86	2.76	4.76E+14	6.89E+26	2.15E+27	5.83%
Conventional	6.30E+14	52.44	32.5	1.71	2.76	5.76E+14	2.93E+27	5.13E+28	-8.60%
Conventional	3.18E+14	16.71	27	1.63	2.76	3.80E+14	3.88E+27	7.32E+27	19.59%
Conventional	2.82E+14	13.08	23.5	1.73	2.76	3.44E+14	3.86E+27	1.48E+28	22.04%
Fuel Blend	5.41E+14	37.78	28.7	1.75	2.76	5.33E+14	5.67E+25	1.89E+28	-1.39%
Fuel Blend	2.62E+14	17.13	27.8	1.71	2.76	2.94E+14	1.01E+27	2.00E+28	12.11%
Fuel Blend	4.15E+14	9.09	20.9	2.03	2.76	1.48E+14	7.16E+28	1.30E+26	-64.46%
Fuel Blend	3.94E+14	20.13	28	1.68	2.76	3.65E+14	8.50E+26	9.18E+25	-7.40%
Fuel Blend	1.78E+14	6.68	26.3	1.68	2.76	1.45E+14	1.10E+27	5.09E+28	-18.66%
Fuel Blend	1.09E+14	4.12	23.4	1.58	2.76	1.59E+14	2.49E+27	8.68E+28	45.81%
						∑	1.24E+29	3.92E+29	$\overline{NMB}$ = 2.37%
							R^2	0.684	

S6.2 FA Model Validation using k_{TEM} & D_{TEM} Coefficients from Boies et al. (2015)

Figure S8 shows the parity plots for the FA model validation when the coefficients k_{TEM} = 0.0125 and D_{TEM} = 0.8 from Boies et al. (2015) are used.

For ground conditions (Figure S8a), estimated EI_n values are in good agreement with measured EI_n from the SAMPLE III.2 (R^2 = 0.963, NMB = +38.9%) experimental campaign. For cruise conditions (Figure S8b), an overall R^2 and NMB values of 0.647 and +6.3% are observed when fitted with the NASA ACCESS data.

However, as mentioned in Section 4.2 in the main text, the R^2 of these validation results are around 2.4% lower, while NMB values are around 32% higher relative to the scenario where k_{TEM} and D_{TEM} coefficients from Dastanpour & Rogak (2014) are used. Therefore, the coefficients from Dastanpour & Rogak (2014) (k_{TEM} = 1.621x10^{-5} & D_{TEM} = 0.39) are used in the final FA model in place of the coefficients from Boies et al. (2015) (k_{TEM} = 0.0125 & D_{TEM} = 0.8).

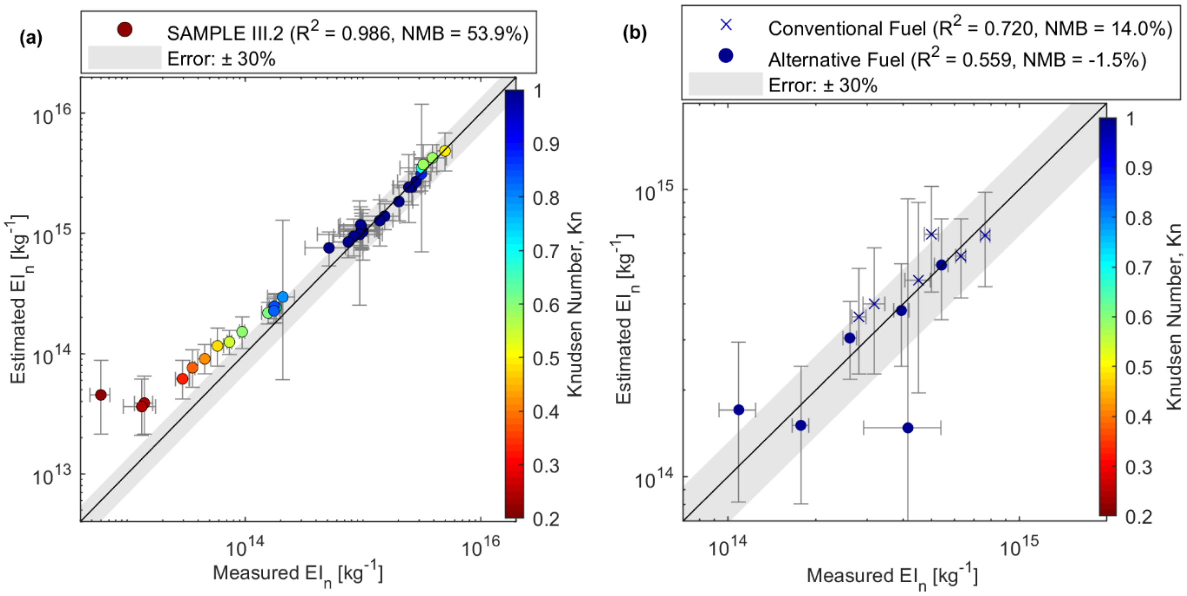

Figure S8: Validation of the FA model for (a) ground conditions using data from Boies et al. (2015), and (b) cruise conditions using data from Moore et al. (2017). k_{TEM} and D_{TEM} prefactor-exponent coefficients specified by Boies et al. (2015), k_{TEM} = 0.0125 & D_{TEM} = 0.8 are used. Horizontal error bars denote random errors from repeated measurements with 1.96σ, and do not include systematic uncertainties from instrumentations.

S6.3 FA Model Validation using Constant k_a = 0.998 & D_α = 1.069 Values from (Eggersdorfer et al., 2012b)

When values of k_a = 0.998 and D_α = 1.069 from Eggersdorfer et al. (2012b) is used to validate the FA model against aircraft emissions at ground (Figure S9a) and cruise (Figure S9b), we obtain an average negative R^2 value and NMB values exceed 100%. An explanation to this phenomenon is provided in Section 4.2 in the main text.

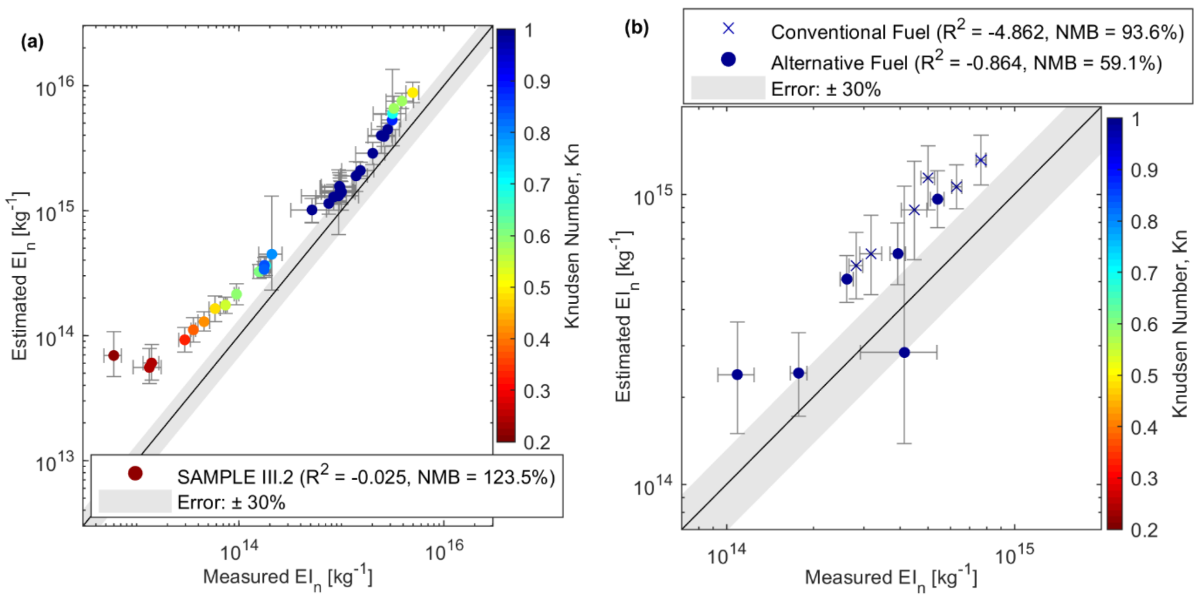

Figure S9: Validation of the FA model for aircraft emissions using constant values of k_a = 0.998 and D_α = 1.069 from Eggersdorfer et al. (2012b) at (a) ground conditions using data from Boies et al. (2015), and (b) cruise conditions using data from Moore et al. (2017). Horizontal error bars denote random errors from repeated measurements with 1.96σ, and do not include systematic uncertainties from instrumentations.

S7 – EXISTING METHODOLOGIES TO ESTIMATE AIRCRAFT BC EI_n

S7.1 Description of Existing Methodologies to Estimate Aircraft BC EI_n

1) EI_n/EI_m Ratio with Altitudinal Variation (Döpelheuer, 2002)

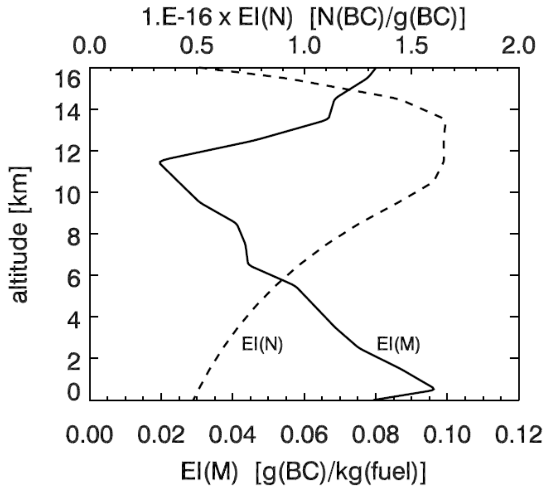

Figure S10: Variation in Aircraft BC EI_m & EI_n vs. altitude (Döpelheuer, 2002; Hendricks et al., 2004).

Note that the EI(N) in Figure S10 denotes BC number-to-mass ratio (number of BC particles emitted per gram of BC), which ranges from 4.8×10^{15} g^{-1}(BC) on the surface to around 1.6×10^{16} g^{-1}(BC) at cruise altitude. A linear interpolation for EI(N) is performed with a 2 km altitude interval prior to applying this methodology to estimate the aircraft BC EI_n.

2) Assumed Particle Diameter (Barrett et al., 2010)

$$M = \frac{\pi}{6}\rho_{\mathrm{NV}} D_{\mathrm{NV}}^3 N_{\mathrm{NV}} \exp\left(\frac{9}{2}(ln\,\sigma_{\mathrm{NV}})^2\right)$$

where: M = EI_m for non-volatile PM (g/kg)
N = EI_n for non-volatile PM (kg^{-1})
Geometric Mean Diameter (GMD) for non-volatile PM, N_{NV} = 38nm
Geometric Standard Deviation (GSD) for non-volatile PM, σ_{NV} = 1.6
Effective Density of non-volatile PM, ρ_{NV} = 1000 kg/m^3

Rearranging for N:

$$N_{\mathrm{NV}} = \frac{M}{1.415\rho_{\mathrm{NV}}D^3}$$

The nominal geometric mean diameter (D_{NV} in this equation) is fixed at 38nm as specified by the authors prior to applying this methodology to estimate the aircraft BC EI_n.

S7.2 Validation of Previous Aircraft BC EI_n Methodologies

Figure S11 shows the ground and cruise validation results for previous BC EI_n estimation methodologies. The average R^2 is 79% lower, and the magnitude of NMB is 90% larger than the FA model presented in Figure 2 (main text). For all data points, the estimated EI_n outputs from Dopelheuer (2002) and Barrett et al. (2010) differ by a constant value. This is due to the assumption of previous methodologies where the BC aggregate property and morphology are fixed and does not capture the variation in the GMD, GSD and D_{fm} versus F/F_{00}.

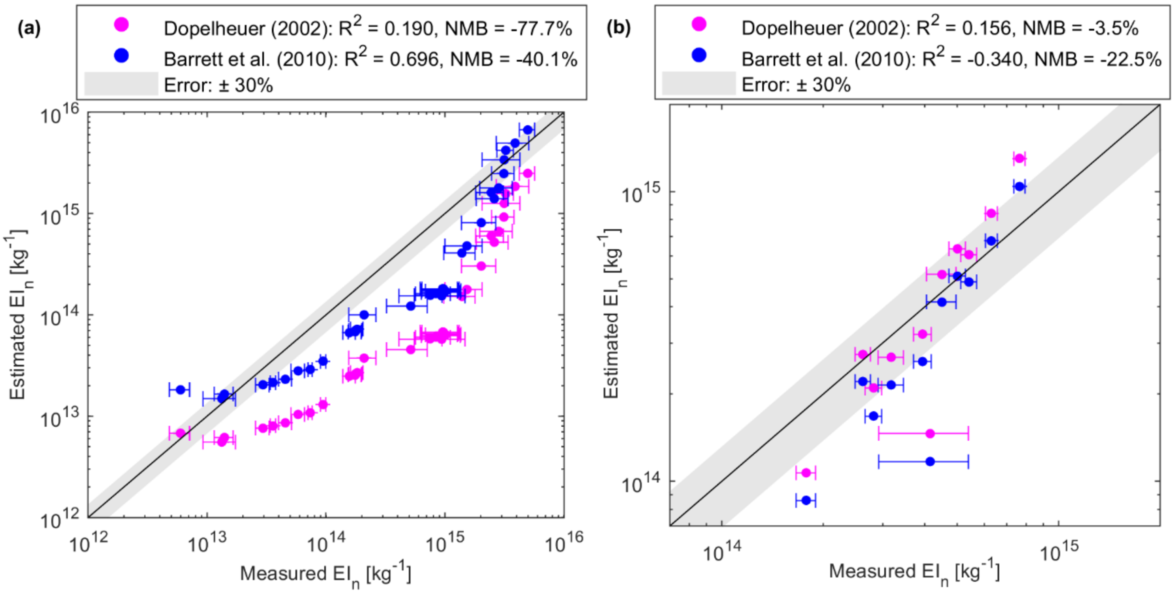

Figure S11: Validation of aircraft BC EI_n for (a) ground and (b) cruise conditions using previous estimation methodologies developed by Dopelheuer (2002) (data points in magenta) and Barrett et al. (2010) (data points in blue). Horizontal error bars denote random errors from repeated measurements with 1.96σ, and do not include systematic uncertainties from instrumentations.

S8 – METHODOLOGY TO ESTIMATE THE KNUDSEN NUMBER (Kn) FOR A GIVEN ENGINE OPERATING CONDITION

According to Hinds (1999), the particle mean free path (λ) is the average distance travelled by a molecule between successive collisions:

$$\lambda = \frac{\bar{c}}{n_z}, \qquad \text{(S6)}$$

where $\bar{c}$ is the mean molecular velocity, or the average distance travelled by the molecule per second. The term n_z is the average number of collisions an air molecule undergoes in one second, which can be expressed as:

$$n_z = \sqrt{2} n \pi {d_m}^2 \bar{c}, \qquad \text{(S7)}$$

where d_m is the diameter of a gas molecule ($d_m = 3.7 \times 10^{-10}\ m$), and n is the number of air molecules per unit volume. Therefore, Eq. S6 and Eq. S7 can be combined:

$$\lambda = \frac{\bar{c}}{\sqrt{2}n\pi {d_m}^2 \bar{c}} \quad \text{(S8)}$$

$$\lambda = \frac{1}{\sqrt{2}n\pi {d_m}^2} \quad \text{(S9)}$$

For a given gas, λ depends only on *n* or gas density:

$$\lambda \propto \frac{1}{n} \qquad \& \qquad n \propto p \quad \text{(S10)}$$

As the number of air molecules per unit volume (*n*) increases, pressure (*p*) increases. Therefore, the particle mean free path of at a given pressure (P_1) can be estimated using standard atmospheric conditions (P_0, λ_0) as a reference:

$$\frac{\lambda_1}{\lambda_0} = \frac{P_0}{P_1} \quad \text{(S11)}$$

$$\lambda_1 = \lambda_0 \frac{P_0}{P_1} \quad \text{(S12)}$$

At standard atmospheric pressure, P_0 = 1 atm, the mean free path, $\lambda_0 = 0.066\ \mu m$. For aircraft engines, the combustion inlet pressure (P_3) is used as the pressure or the closest region where BC particles are formed. The formulas required to calculate P_3 can be found in Cumpsty (2003) and Stettler et al. (2013a). Similarly, the gross indicated mean effective pressure (GIMEP) is used for the CIDI internal combustion engine (Graves et al., 2015), while BC is assumed to form under one atmospheric pressure for the soot generator.

The Knudsen Number (Kn) is a dimensionless number equal to the ratio of the mean free path to the particle radius:

$$\mathrm{Kn} = \frac{2\lambda}{d} \quad \text{(S13)}$$

According to Sorensen (2011), the continuum regime starts when $\mathrm{Kn} \leq 1$, while the transition regime is when $0.1 < \mathrm{Kn} < 10$. Finally, the free-molecular regime is when $\mathrm{Kn} \geq 1$. To use Eq. S13 to estimate the Kn, the mean free path (λ) can be estimated using Eq. S12, while particle diameter (*d*) can be estimated using the GMD.

The Knudsen number (Kn) for each data point is estimated for the CIDI internal combustion engine (Table S10), soot generator (Table S11) and the two aircraft BC emissions dataset at ground (Table S12) and cruise conditions (Table S13).

For BC aggregates produced from the soot generator, 77% of the data points form in the free-molecular regime (Kn > 1) as P_1 is at one atmosphere and the Kn primarily depends on the BC GMD. A larger GMD contributes to a lower Kn because the Kn and GMD are inversely proportional (Eq. S13). For the CIDI and aircraft gas turbine engine on the ground, BC aggregates are increasingly formed in the continuum and transition regime (Kn < 1) at higher engine operating conditions. 92% of the BC aggregates are formed in the free-molecular regime (Kn > 1) when the gas turbine engine is operating at cruise conditions, which explanations to this phenomenon is provided in Section 4.2 in the main text.

Table S10: Knudsen number calculations for each data point in the CIDI dataset.

Engine Mode	GIMEP (atm)	GMD (nm)	λ_1 (μm)	Kn
B75 20% EGR	16.28	90.01	0.004	0.090
	16.28	86.55	0.004	0.094
	16.28	84.69	0.004	0.096
B75 0% EGR	10.86	63.07	0.006	0.209
	10.86	65.72	0.006	0.213
B50 20% EGR	8.14	58.02	0.008	0.442
	8.14	56.97	0.008	0.338
B37 20% EGR	8.14	36.66	0.008	0.411
	8.14	47.91	0.008	0.424
	5.43	39.5	0.012	0.775
	5.43	38.26	0.012	0.802
B25 20% EGR	5.43	31.38	0.012	0.795
	13.6784	30.31	0.005	0.154
	13.6784	30.56	0.005	0.155
A63 80% Premixed	16.28	62.8	0.004	0.129
	16.28	62.36	0.004	0.123

Table S11: Knudsen number calculations for each data point from the soot generator.

Sample	P_1 (atm)	GMD (nm)	λ_1 (μm)	Kn
1	1	41.62	0.066	3.171
2	1	111.92	0.066	1.179
3	1	128.78	0.066	1.025
4	1	40.73	0.066	3.241
5	1	124.62	0.066	1.059
6	1	147.08	0.066	0.897
7	1	143.35	0.066	0.921
8	1	85.42	0.066	1.545
9	1	120.43	0.066	1.096
10	1	145.40	0.066	0.908
11	1	42.39	0.066	3.114
12	1	80.31	0.066	1.644
13	1	127.69	0.066	1.034

Table S12: Knudsen number calculations for each data point for the aircraft gas turbine engine (ground).

F/F_{00} (%)	P_1 (atm)	GMD (nm)	λ_1 (μm)	Kn	F/F_{00} (%)	P_3 (atm)	GMD (nm)	λ_1 (μm)	Kn
3.3%	1.885	16.088	0.035	4.352	41.1%	11.980	18.486	0.006	0.596
3.3%	1.882	15.894	0.035	4.413	45.8%	13.216	18.581	0.005	0.538
3.3%	1.881	15.875	0.035	4.421	51.1%	14.642	18.848	0.005	0.478
3.3%	1.884	15.903	0.035	4.405	57.1%	16.245	19.169	0.004	0.424
3.3%	1.882	15.958	0.035	4.395	62.9%	17.797	19.739	0.004	0.376
3.3%	1.884	15.972	0.035	4.386	69.1%	19.459	20.726	0.003	0.327
3.3%	1.885	15.928	0.035	4.396	85.7%	23.882	22.748	0.003	0.243
3.3%	1.883	15.941	0.035	4.399	94.6%	26.258	22.897	0.003	0.220
7.6%	3.034	21.155	0.022	2.057	84.3%	23.517	23.000	0.003	0.244
9.4%	3.502	23.248	0.019	1.621	3.3%	1.885	16.259	0.035	4.306
11.2%	3.991	25.772	0.017	1.283	3.4%	1.903	16.443	0.035	4.219
13.3%	4.549	27.285	0.015	1.064	6.6%	2.749	20.813	0.024	2.307
15.5%	5.140	29.231	0.013	0.879	9.8%	3.604	24.343	0.018	1.505
17.7%	5.725	33.523	0.012	0.688	13.3%	4.538	27.502	0.015	1.058
20.5%	6.476	35.019	0.010	0.582	20.5%	6.479	34.703	0.010	0.587
23.3%	7.228	37.448	0.009	0.488	26.4%	8.061	19.464	0.008	0.841
26.4%	8.045	20.586	0.008	0.797	3.4%	1.918	17.299	0.034	3.978
33.1%	9.827	19.575	0.007	0.686	26.8%	8.152	19.489	0.008	0.831
36.9%	10.844	19.888	0.006	0.612					

Table S13: Knudsen number calculations for each data point for the aircraft gas turbine engine (cruise).

F/F_{00} (%)	Mach No.	P_1 (Pa)	GMD (nm)	λ_1 (μm)	Kn
41.7%	0.840	391157	35.3	0.017	0.969
31.3%	0.725	270863	29.7	0.025	1.663
25.8%	0.600	206179	25.5	0.032	2.544
41.7%	0.840	391157	32.5	0.017	1.052
31.3%	0.725	270863	27.0	0.025	1.829
25.8%	0.600	206179	23.5	0.032	2.760
41.7%	0.840	391157	28.7	0.017	1.191
31.3%	0.725	270863	27.8	0.025	1.776
25.8%	0.600	206179	20.9	0.032	3.104
41.7%	0.840	391157	28.0	0.017	1.221
31.3%	0.725	270863	26.3	0.025	1.878
25.8%	0.600	206179	23.4	0.032	2.772

S9 – UNCERTAINTY AND SENSITIVITY ANALYSIS

S9.1 Uncertainty Quantification for Different Measuring Instruments and Input Parameters of the FA Model

For all the uncertainty and sensitivity analysis conducted in this study:

- All uncertainties are reported with a 95% confidence interval (1.96σ).
- Systematic uncertainties are denoted as $\frac{B_x}{|x|}$
- Precision uncertainties are denoted as $\frac{P_x}{|x|}$
- Total uncertainties (Systematic + Precision) are denoted as $\frac{T_x}{|x|}$

- The systematic and/or precision uncertainties for each parameter that are included in this analysis depends on data availability.
- Uncertainties in penetration efficiencies & thermophoresis losses are not included, similar to Olfert et al. (2017).

The following list are systematic uncertainties from different aerosol measuring instruments that were obtained from the literature:

- Uncertainty in DMA measurements = 3% (Kinney et al., 1991)
- Uncertainty in CPC measurements = 2.8% (Owen et al., 2012)
- Uncertainty in CPMA measurements = 4% (Olfert et al., 2017)
- Uncertainty in LII measurements = 25% (Boies et al., 2015)

If multiple instruments are required to measure a parameter, the root-sum-square (RSS) method is used to combine the systematic uncertainties arising from different measuring instruments to estimate the total uncertainty of the measured *N*, *M*, GMD and GSD:

1) <u>Total Uncertainty in Measured *N*</u>

$N = \sum_{i=1}^{n} n_i$

where n_i is measured with an SMPS (DMA-CPC), or directly from a CPC.

- Only uncertainties from the CPC is used. Uncertainties introduced by the DMA (on measurements of d_m) are excluded because the number of particles will still be counted even if d_m measurements are inaccurate, provided that the entire particle size distribution is scanned.

$$\frac{T_N}{|N|} = 2.8\%$$

2) <u>Systematic/Total Uncertainty in Measured *M*</u>

i. If *M* is estimated with the IPSD method (DMA-CPMA-CPC), M_{IPSD}:
Using the RSS Method, systematic uncertainties for each variable in Eq. S4 ($M_{IPSD} = \sum_{i=1}^{j} n_i (\rho_{eff})_i (\frac{\pi}{6} {d_m}^3)_i$) are propagated to estimate the uncertainties for M_{IPSD} where:

- n_i is measured with a CPC, $\frac{B_n}{|n|} = 2.8\%$

- Effective density, $\rho_{eff} = \frac{m}{\frac{\pi}{6}{d_m}^3}$ is estimated with a DMA to obtain d_m ($\frac{B_{d_m}}{|d_m|} = 3\%$), and a CPMA to measure m ($\frac{B_m}{|m|} = 4\%$). Hence, based on the RSS method: $\frac{B_{\rho_{eff}}}{|\rho_{eff}|} = \sqrt{0.04^2 + (3 \times 0.03)^2} = 9.8\%$

Therefore, the systematic uncertainty of M (DMA-CPMA-CPC) is:

$$\frac{B_{M_{IPSD}}}{|M_{IPSD}|} = \sqrt{0.098^2 + (3 \times 0.03^2) + 0.028^2} = 11.4\%$$

ii. If M is measured with a laser-induced incandescence (LII), M_LII, the uncertainty value quoted in the SI of Boies et al. (2015) is:

$$\frac{T_{M_\mathrm{LII}}}{|M_\mathrm{LII}|} = 25\%$$

3) <u>Total Uncertainty in D_fm</u>

Using average standard deviation values from Abegglen et al. (2015), $\frac{T_{D_\mathrm{fm}}}{|D_\mathrm{fm}|} = 7.88\%$

4) <u>Total Uncertainty in BC ρ_0</u>

BC ρ_0 = 1770 ± 70 kg/m^3 (Park et al., 2004). Hence, $\frac{T_{\rho_0}}{|\rho_0|} = \frac{70}{1770} \times 1.96 = 7.75\%$

5) <u>Systematic Uncertainty in the Measured GMD</u>

The GMD of a BC particle size distribution is calculated using Eq. S1(GMD $= \exp\left(\frac{\sum n_i \ln(d_i)}{N}\right)$), where:

- $\frac{B_n}{|n|}$ and $\frac{B_N}{|N|} = 2.8\%$,
- $\frac{B_{d_m}}{|d_m|} = 3\%$.

Using the RSS Method: $\frac{B_\mathrm{GMD}}{|\mathrm{GMD}|} = \sqrt{0.028^2 + 0.028^2 + 0.03^2} = 4.97\%$

However, the RSS method does not account for additional uncertainties resulting from the inversion method, bipolar diffusion charging and the DMA transfer function. Hence, we have increased the uncertainties of the GMD to the maximum tolerable uncertainty of ± 10% according to the calibration standards specified by the European Center for Aerosol Calibration (ECAC) and the World Calibration Center for Aerosol Physics (WCCAP) (Wiedensohler et al., 2018).

$$\text{Therefore, } \frac{B_\mathrm{GMD}}{|\mathrm{GMD}|} = 10\%$$

6) Systematic Uncertainty in Measured GSD

Similar to the uncertainties in the measured GMD, an uncertainty of ± 10% is specified for the measured GSD, which is in accordance to the calibration standards of the ECAC and WCCAP (Wiedensohler et al., 2018).

$$\text{Therefore, } \frac{B_{\mathrm{GSD}}}{|\mathrm{GSD}|} = 10\%$$

Next, systematic uncertainties for k_{TEM} and D_{TEM} is estimated using the 95% confidence intervals published in the SI of Dastanpour & Rogak (2014):

7) Systematic Uncertainty in k_{TEM}

Source	LB k_{TEM}	Mean k_{TEM}	UB k_{TEM}	% Diff (LB)	% Diff (UB)
GDI	2.165E-06	2.616E-06	3.067E-06	17.24%	17.24%
HPDI	2.224E-06	2.644E-06	3.063E-06	15.87%	15.87%
Aviation gas turbine	1.087E-05	1.621E-05	2.155E-05	32.93%	32.93%
Inverted burner	1.198E-06	2.465E-06	3.736E-06	51.40%	51.57%
			Avg	29.36%	29.40%

- For CIDI/HPDI internal combustion engines, $\frac{B_{k_{\mathrm{TEM}}}}{|k_{\mathrm{TEM}}|} = 15.9\%$
- For aircraft gas turbine engines, $\frac{B_{k_{\mathrm{TEM}}}}{|k_{\mathrm{TEM}}|} = 32.9\%$

8) Systematic Uncertainty in D_{TEM}

Source	Mean D_{TEM}	LB D_{TEM}	UB D_{TEM}	% Diff (LB)	% Diff (UB)
GDI	0.30	0.26	0.33	13.33%	10.00%
HPDI	0.29	0.26	0.32	10.34%	10.34%
Aviation gas turbine	0.39	0.32	0.46	17.95%	17.95%
Inverted burner	0.29	0.20	0.38	31.03%	31.03%
			Avg	18.17%	17.33%

- For CIDI/HPDI internal combustion engines, $\frac{B_{D_{\mathrm{TEM}}}}{|D_{\mathrm{TEM}}|} = 10.3\%$
- For aircraft gas turbine engines, $\frac{B_{D_{\mathrm{TEM}}}}{|D_{\mathrm{TEM}}|} = 18.0\%$

The precision uncertainties of k_a and D_α are estimated using numerical simulation results from Eggersdorfer & Pratsinis (2012):

9) Precision Uncertainty in k_a

$$\frac{P_{k_a}}{|k_a|} = 1.2\%$$

10) Precision Uncertainty in D_α

$$\frac{P_{D_\alpha}}{|D_\alpha|} = 0.3\%$$

Finally, given that the uncertainty distribution for C_{ov} is not known, we assume that C_{ov} is uniformly distributed according to the range given by Bourrous et al. (2018) ($0.02 \leq C_{ov} \leq 0.24$). Overall, the uncertainties for the different model input parameters required for the FA model are summarised in Table S14.

Table S14: A summary of the systematic or precision uncertainties for the different model input parameters required for the FA model.

Systematic/Bias Uncertainty (1.96σ)		Precision Uncertainty (1.96σ)		Total Uncertainty (1.96σ)	
Input	**Uncertainty**	**Input**	**Uncertainty**	**Input**	**Uncertainty**
M_{IPSD}	± 11.4%	k_a	± 1.20%	N_{CPC}	± 2.8%
GMD	± 10%	D_α	± 0.30%	M_{LII}	± 25%
GSD	± 10%			D_{fm}	± 7.88%
k_{TEM}	± 29.4% (Avg)			ρ_0	± 7.75%
D_{TEM}	± 17.8% (Avg)				

- Uncertainty range for C_{ov} ~ U[0.02, 0.24]

S9.2 Uncertainty Quantification for the FA Model Output

The uncertainty for the FA model output (estimated N or EI_n) is quantified using a numerical Monte Carlo 1000-member ensemble due to the non-linear properties of the FA model with higher-order components, as well as the potential presence of covariance between input variables. Absolute values required for this Monte Carlo method were measured from the SAMPLE III.2 campaign (using the data point at $F/F_{00} = 0.4$). Table S15 summarises the absolute values and its associated uncertainties, and the uncertainty for each model input variable was described in the previous subsection, S9.1.

Table S15: Absolute values (from the SAMPLE III.2 dataset) and the associated uncertainties for each model input variables to be used in the Monte Carlo Method to estimate the uncertainty of the FA model output, the estimated EI_n.

Variable	Fixed F/F_{00}	Uncertainty Distribution	Mean (μ)	Std Dev (1.96σ)
EI_m (LII)	0.4	Normal Distribution	2.7 mg/kg	25% × μ
$\boldsymbol{\rho_0}$			1770 kg/m^3	70 kg/m^3
k_a			1	1.2% × μ
D_{fm}			2.76	7.9% × μ
k_{TEM}			1.621x10^{-5}	32.9% × μ
D_{TEM}			0.39	18% × μ
GMD			18.49 nm	10% × μ
GSD			1.73	10% × μ
C_{ov}		Uniform Distribution	[0.02, 0.24]	

After 10000 iterations, the Monte Carlo simulation is stopped when differences in the uncertainty estimates between model runs converge to below 1% (Coleman & Steele, 2009), as shown in Figure S12. The procedure specified by Coleman & Steele (2009) was used to determine the 95% probabilistic systematic coverage interval and the associated uncertainty limits of the FA model outputs:

1) Sort the M_{MCM} number of Monte Carlo outputs (M_{MCM} = 10000 runs), the estimated EI_n outputs from the lowest to the highest value.

2) For a 95% coverage interval:
   - EI_n lower bound, r_{low} = result number ($0.025 M_{MCM}$) = 6.655×10^{13}
   - EI_n upper bound, r_{high} = result number ($0.975\ M_{MCM}$) = 2.915×10^{14}

3) For 95% expanded uncertainty limits:
   - $U_r^- = r(X_1, X_2, \ldots X_J) - r_{\mathrm{low}} = 7.736 \times 10^{13}$ (- 53.8%)
   - $U_r^+ = r_{\mathrm{high}} - r(X_1, X_2, \ldots X_J) = 1.476 \times 10^{14}$ (+102.5%)

4) The interval that contains $EI_{n,true}$ at a 95% confidence level:
   - $r - U_r^- \leq r_{\mathrm{true}} \leq r + U_r^+$
   - $7.736 \times 10^{13} \leq \mathrm{EI}_{\mathrm{n,true}} \leq 1.476 \times 10^{14}$
   - Therefore, $\mathrm{EI}_{\mathrm{n}} = (1.439 \times 10^{14}) \times (-53.8\%, +102.5\%)\mu$

Using the Monte Carlo method, Figure S13a shows an asymmetrical distribution of the FA model outputs (the estimated EI_n) with an uncertainty bound of $(-54\%, +103\%) \times \mu$ at 1.96σ. This asymmetrical distribution is due to the non-linearity of the FA model and the large uncertainties for most input variables (>5%) (Coleman & Steele, 2009).

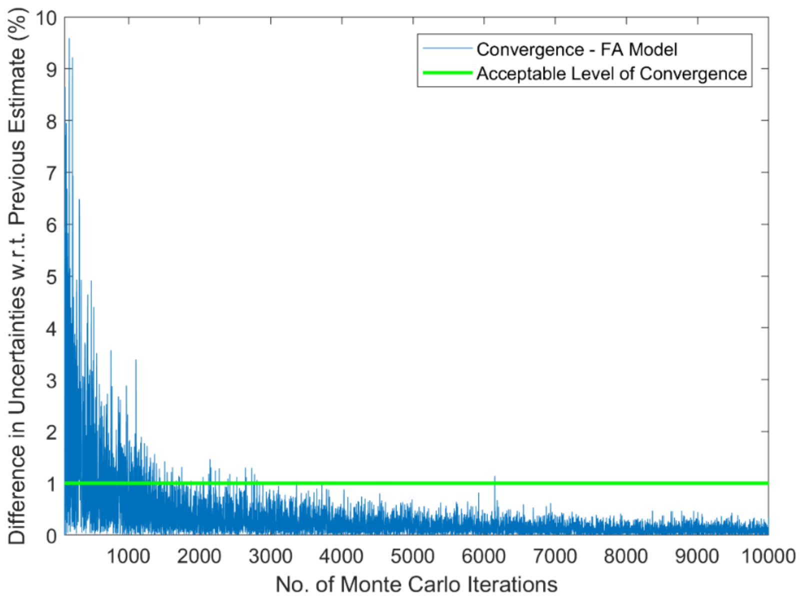

Figure S12: Convergence of the uncertainties of the FA model outputs (the estimated EI_n) relative to the number of iterations for the Monte Carlo Method. After 1000 iterations, the percentage difference in uncertainties relative to previous estimates generally fall below 1%.

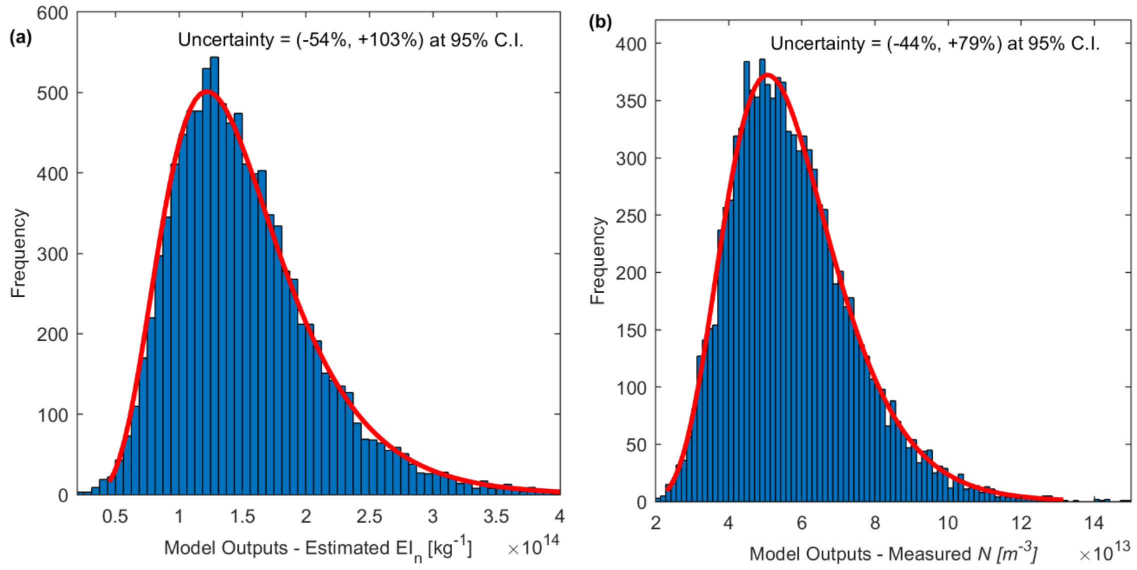

Figure S13: Distribution of the FA model outputs (the estimated N or EI_n) using the Monte Carlo Method with absolute values from (a) the SAMPLE III.2 aircraft emissions dataset (ground level) from Boies et al. (2015), and (b) the CIDI engine dataset from Graves et al. (2015).

To check the consistency of the uncertainty bounds of the FA model outputs, the Monte Carlo method is rerun with the dataset from the CIDI internal combustion engine (Graves et al., 2015), where the absolute values and associated uncertainties are listed in Table S16. Overall, the uncertainty bound of the FA model output estimated with data from the CIDI engine $(-44\%, +79\%) \times \mu$ at 1.96σ (Figure S13b) is slightly lower than the uncertainties of an aircraft gas turbine engine because of the lower uncertainty values of M_{IPSD} (± 11.4%), k_{TEM} (± 15.9%) and D_{TEM} (± 10.3%).

Table S16: Absolute values (from the CIDI dataset of Graves et al. (2015)) and the associated uncertainties for each model input variables to be used in the Monte Carlo Method to estimate the uncertainty of the FA model output, the estimated *N*.

Variable	Fixed Engine Operating Condition	Uncertainty Distribution	Mean (μ)	Std Dev (σ)
M_{IPSD}	B75, 20% EGR	Normal Distribution	1.80×10^{-5} kg/m³	11.4% × μ
$\boldsymbol{\rho_0}$			1770 kg/m³	70
k_a			0.83	1.2% × μ
D_α			1.08	0.3% × μ
k_{TEM}			2.64×10^{-6}	6.67% × μ
D_{TEM}			0.29	7.9% × μ
GMD			90.01 nm	4.97% × μ
GSD			1.573	6.13% × μ
C_{ov}		Uniform DIstribution	[0.02, 0.24]	

S9.3 Sensitivity Analysis for the FA Model

Figure S14 presents the results of the variance-based global sensitivity analysis on the FA model. The total-effect index (S_{Ti}) identifies the total contribution of each input parameters to the variance of the FA model output, where higher-order interactions between variables are also accounted for (Saltelli et al., 2008). Due to the non-linear and non-additive properties of the FA model, the summation of S_{Ti} for each input variable is greater than one.

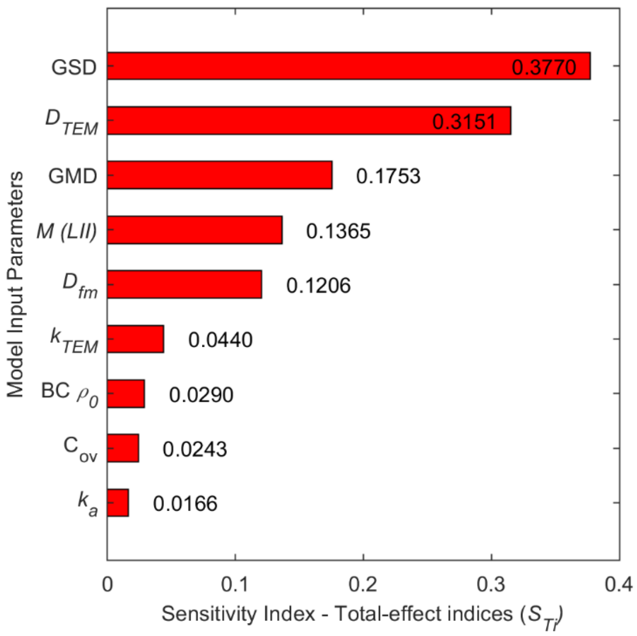

Figure S14: Total Effect Sensitivity Analysis for the FA model input parameters. Data tables, as well as the specification of μ (measured with the SAMPLE III.2 dataset from Boies et al. (2015)) and σ for each input variable can be found in Table S15.

END OF SUPPLEMENTARY INFORMATION

References

Abegglen, M., Durdina, L., Brem, B. T., Wang, J., Rindlisbacher, T., Corbin, J. C., … Sierau, B. (2015). Effective density and mass-mobility exponents of particulate matter in aircraft turbine exhaust: Dependence on engine thrust and particle size. *Journal of Aerosol Science*, *88*, 135–147. https://doi.org/10.1016/j.jaerosci.2015.06.003

Barrett, S. R. H., Prather, M., Penner, J., Selkirk, H., Balasubramanian, S., Döpelheuer, A., … Hileman, J. (2010). Guidance on the use of AEDT gridded aircraft emissions in atmospheric models. *US Federal Aviation Administration Office of Environment and Energy*.

Boies, A. M., Stettler, M. E. J., Swanson, J. J., Johnson, T. J., Olfert, J. S., Johnson, M., … Thomson, K. (2015). Particle emission characteristics of a gas turbine with a double annular combustor. *Aerosol Science and Technology*, *49*(9), 842–855.

Bourrous, S., Ribeyre, Q., Lintis, L., Yon, J., Bau, S., Thomas, D., … Ouf, F.-X. (2018). A semi-automatic analysis tool for the determination of primary particle size, overlap coefficient and specific surface area of nanoparticles aggregates. *Journal of Aerosol Science*, *126*, 122–132.

Brasil, A. M., Farias, T. L., & Carvalho, M. G. (1999). A recipe for image characterization of fractal-like aggregates. *Journal of Aerosol Science*, *30*(10), 1379–1389.

Coleman, H. W., & Steele, W. G. (2009). *Experimentation, validation, and uncertainty analysis for engineers*. John Wiley & Sons.

Cumpsty, N. (2003). Jet Propulsion. A simple guide to the aerodynamic and thermodynamic design and performance of jet engines. Second Edition, *1*, 13.

Dastanpour, R., & Rogak, S. N. (2014). Observations of a correlation between primary particle and aggregate size for soot particles. *Aerosol Science and Technology*, *48*(10), 1043–1049.

Dastanpour, R., Rogak, S. N., Graves, B., Olfert, J., Eggersdorfer, M. L., & Boies, A. M. (2016). Improved sizing of soot primary particles using mass-mobility measurements. *Aerosol Science and Technology*, *50*(2), 101–109.

Döpelheuer, A. (2002). No Title. *Anwendungsorientierte Verfahren Zur Bestimmung von CO, HC Und Ruß Aus Luftfahrttriebwerken*.

Durdina, L., Brem, B. T., Abegglen, M., Lobo, P., Rindlisbacher, T., Thomson, K. A., … Wang, J. (2014). Determination of PM mass emissions from an aircraft turbine engine using particle effective density. *Atmospheric Environment*, *99*, 500–507.

Eggersdorfer, M. L., Gröhn, A. J., Sorensen, C. M., McMurry, P. H., & Pratsinis, S. E. (2012a). Mass-mobility characterization of flame-made ZrO 2 aerosols: Primary particle diameter and extent of aggregation. *Journal of Colloid and Interface Science*, *387*(1), 12–23.

Eggersdorfer, M. L., Kadau, D., Herrmann, H. J., & Pratsinis, S. E. (2012b). Aggregate morphology evolution by sintering: number and diameter of primary particles. *Journal of Aerosol Science*, *46*, 7–19.

Eggersdorfer, M. L., & Pratsinis, S. E. (2012). The structure of agglomerates consisting of polydisperse particles. *Aerosol Science and Technology*, *46*(3), 347–353.

EU. (1999). Directive 1999/96/EC of the European Parliament and of the Council of 13 December 1999 on the approximation of the laws of the Member States relating to measures to be taken against the emission of gaseous and particulate pollutants from compression ignit. Retrieved from https://publications.europa.eu/en/publication-detail/-/publication/1246686e-7169-4f7b-a4c5-41034e3269f9/language-en

Gormley, P. G., & Kennedy, M. (1948). Diffusion from a stream flowing through a cylindrical tube. In *Proceedings of the Royal Irish Academy. Section A: Mathematical and Physical Sciences* (pp. 163–169). JSTOR.

Graves, B., Olfert, J., Patychuk, B., Dastanpour, R., & Rogak, S. (2015). Characterization of particulate matter morphology and volatility from a compression-ignition natural-gas direct-injection engine. *Aerosol Science and Technology*, *49*(8), 589–598.

Hendricks, J., Kärcher, B., Döpelheuer, A., Feichter, J., Lohmann, U., & Baumgardner, D. (2004). Simulating the global atmospheric black carbon cycle: a revisit to the contribution of aircraft emissions. *Atmospheric Chemistry and Physics*, *4*(11/12), 2521–2541.

Hinds, W. C. (1999). Aerosol Technology: Properties. *Behavior, and Measurement of Airborne Particles (2nd*.

Johnson, T. J., Olfert, J. S., Symonds, J. P. R., Johnson, M., Rindlisbacher, T., Swanson, J. J., … Walters, D. (2015). Effective density and mass-mobility exponent of aircraft turbine particulate matter. *Journal of Propulsion and Power*, *31*(2), 573–582.

Kinney, P. D., Pui, D. Y. H., Mulliolland, G. W., & Bryner, N. P. (1991). Use of the electrostatic classification method to size 0.1 μm SRM particles—a feasibility study. *Journal of Research of the National Institute of Standards and Technology*, *96*(2), 147.

Liati, A., Brem, B. T., Durdina, L., Vögtli, M., Arroyo Rojas Dasilva, Y., Dimopoulos Eggenschwiler, P., & Wang, J. (2014). Electron microscopic study of soot particulate matter emissions from aircraft turbine engines. *Environmental Science & Technology*, *48*(18), 10975–10983.

Liu, Z. G., Vasys, V. N., Dettmann, M. E., Schauer, J. J., Kittelson, D. B., & Swanson, J. (2009). Comparison of strategies for the measurement of mass emissions from diesel engines emitting ultra-low levels of particulate matter. *Aerosol Science and Technology*, *43*(11), 1142–1152.

Lobo, P., Hagen, D. E., Whitefield, P. D., & Raper, D. (2015). PM emissions measurements of in-service commercial aircraft engines during the Delta-Atlanta Hartsfield Study. *Atmospheric Environment*, *104*, 237–245.

Magnus, W., Oberhettinger, F., & Soni, R. (2013). *Formulas and theorems for the special functions of mathematical physics* (Vol. 52). Springer Science & Business Media.

Moore, R. H., Thornhill, K. L., Weinzierl, B., Sauer, D., D'Ascoli, E., Kim, J., … Beyersdorf, A. J. (2017). Biofuel blending reduces particle emissions from aircraft engines at cruise conditions. *Nature*, *543*(7645), 411–415.

Moran, J., Cuevas, J., Liu, F., Yon, J., & Fuentes, A. (2018). Influence of primary particle polydispersity and overlapping on soot morphological parameters derived from numerical TEM images. *Powder Technology, 330*, 67–79.

Olfert, J. S., Dickau, M., Momenimovahed, A., Saffaripour, M., Thomson, K., Smallwood, G., … Crayford, A. (2017). Effective density and volatility of particles sampled from a helicopter gas turbine engine. *Aerosol Science and Technology*, *51*(6), 704–714.

Owen, M., Mulholland, G., & Guthrie, W. (2012). Condensation Particle Counter Proportionality Calibration from 1 particle· cm− 3 to 104 particles· cm− 3. *Aerosol Science and Technology*, *46*(4), 444–450.

Park, K., Kittelson, D. B., Zachariah, M. R., & McMurry, P. H. (2004). Measurement of inherent material density of nanoparticle agglomerates. *Journal of Nanoparticle Research*, *6*(2), 267–272.

Saltelli, A., Ratto, M., Andres, T., Campolongo, F., Cariboni, J., Gatelli, D., … Tarantola, S. (2008). *Global sensitivity analysis: the primer*. John Wiley & Sons.

Sorensen, C. M. (2011). The mobility of fractal aggregates: a review. *Aerosol Science and Technology*, *45*(7), 765–779.

Stettler, M., & Boies, A. (2014). Aircraft non-volatile particle emissions: estimating number from mass. In *18th ETH Conference on Combustion Generated Nanoparticles*. Zurich, Switzerland: ETH Zurich. https://doi.org/10.1016/j.atmosenv.2009.06.005

Stettler, M. E. J., Boies, A., Petzold, A., & Barrett, S. R. H. (2013a). Global civil aviation black carbon emissions. *Environmental Science & Technology*, *47*(18), 10397–10404.

Stettler, M. E. J., Swanson, J. J., Barrett, S. R. H., & Boies, A. M. (2013b). Updated correlation between aircraft smoke number and black carbon concentration. *Aerosol Science and Technology*, *47*(11), 1205–1214.

Stettler, M., Teoh, R., & Schumann, U. (2017). Aircraft Black Carbon Particle Number Emissions-New Predictive Method & Uncertainty Analysis. In *Cambridge Particle Meeting 2017*. Cambridge, United Kingdom: Department of Engineering, University of Cambridge. https://doi.org/10.1002/2015JD024696

Teoh, R., Stettler, M., & Majumdar, A. (2017). Aircraft black carbon particle number emissions—a new predictive method and uncertainty analysis. In *21st ETH-Conference on Combustion Generated Naniparticles*. Zurich, Switzerland: ETH Zurich. Retrieved from http://www.nanoparticles.ch/archive/2017_Teoh_PO.pdf

Teoh, R., Stettler, M., Majumdar, A., & Schumann, U. (2018a). A Methodology to Relate Black Carbon Particle Number and Mass Emissions from Various Combustion Sources. In *Cambridge Particle Meeting 2018*. Cambridge, United Kingdom: Department of Engineering, University of Cambridge. Retrieved from http://www.cambridgeparticlemeeting.org/sites/default/files/Presentations/2018/CPM_Teoh_2018_Methodology to Relate Black Carbon Particle Number and Mass Emissions.pdf

Teoh, R., Stettler, M., Majumdar, A., & Schumann, U. (2018b). A Methodology to Relate Black Carbon Particle Number and Mass Emissions from Various Combustion Sources. In *22nd ETH-Conference on Combustion Generated Nanoparticles, June 18th - 21st.* Zurich, Switzerland: ETH Zurich. Retrieved from http://www.nanoparticles.ch/archive/2018_Teoh_PO.pdf

Timko, M. T., Onasch, T. B., Northway, M. J., Jayne, J. T., Canagaratna, M. R., Herndon, S. C., … Knighton, W. B. (2010). Gas turbine engine emissions—Part II: Chemical properties of particulate matter. *Journal of Engineering for Gas Turbines and Power*, *132*(6), 61505.

Wey, C. C., Anderson, B. E., Hudgins, C., Wey, C., Li-Jones, X., Winstead, E., … Whitefield, P. (2006). Aircraft particle emissions experiment (APEX).

Wiedensohler, A., Wiesner, A., Weinhold, K., Birmili, W., Hermann, M., Merkel, M., … Tuch, T. (2018). Mobility particle size spectrometers: Calibration procedures and measurement uncertainties. *Aerosol Science and Technology*, *52*(2), 146–164.